Electronic Supplementary Material (ESI) for Dalton Transactions.

Supporting Information

Tris(2-pyridylmethyl)amine-ligated Cu(II) 1,3-diketonate complexes: Anaerobic retro-Claisen and dehalogenation reactivity of 2-chloro-1,3-diketonate derivatives

Josiah G. D. Elsberg,[a], Stephen N. Anderson.[a] David L. Tierney,[b] Eric W. Reinheimer[c]
and Lisa M. Berreau[a,]*

[a]Department of Chemistry & Biochemistry, Utah State University, 0300 Old Main Hill, Logan, UT 84322-0300, USA

[b]Department of Chemistry and Biochemistry, Miami University, Oxford, OH 45056, USA

[c]Rigaku Americas Corporation, 9009 New Trails Drive, The Woodlands, TX 77381, USA

Contact information:

Lisa M. Berreau

lisa.berreau@usu.edu

Table of Contents

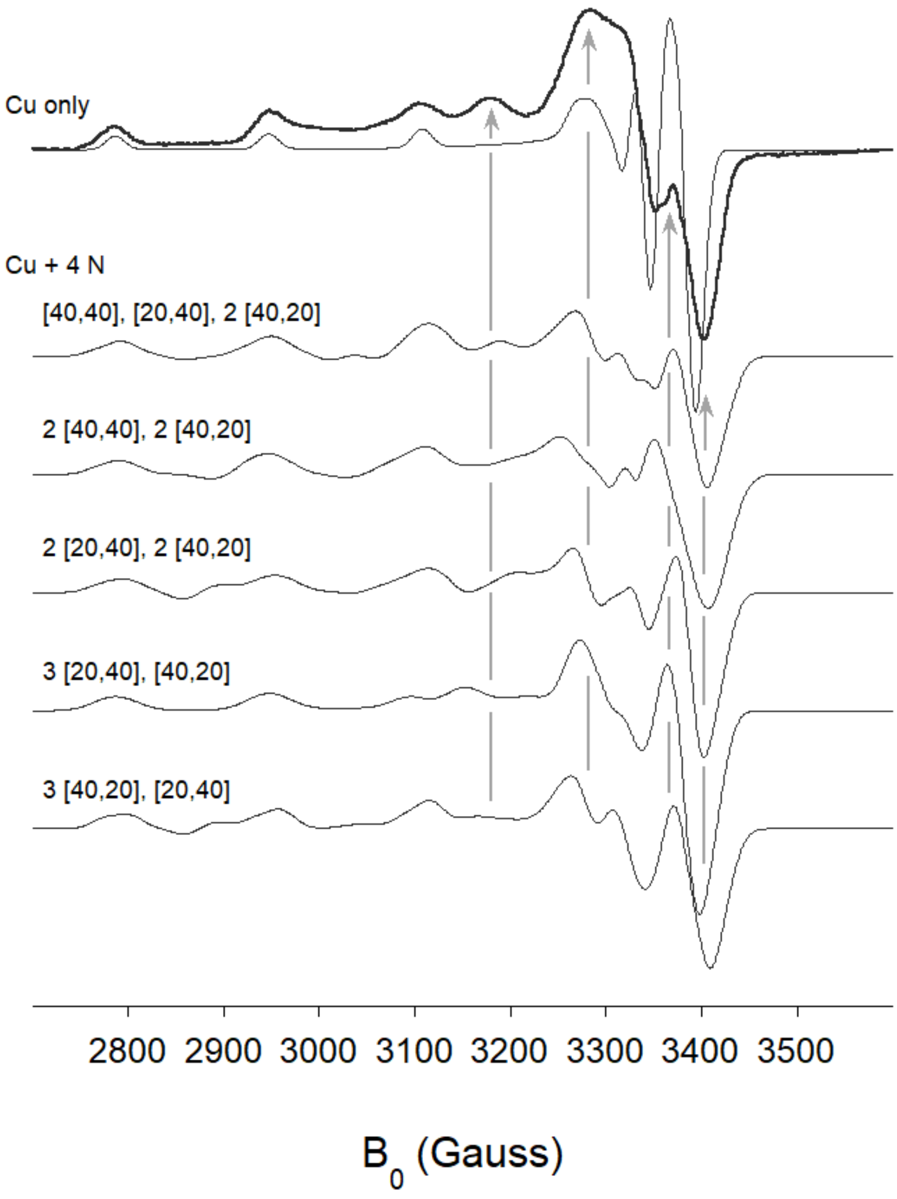

Figure S1. EPR simulations for **3-5**. As the data do not contain sufficient resolution to simultaneously determine five hyperfine tensors, to add in the ^{14}N couplings, we initially limited the possible ^{14}N hyperfine tensors to $[A_{||}, A_{\perp}]$ = [20, 40] or [40, 20] MHz, depending on whether the nitrogen in question was in the xy-plane or on the z-axis (M. Iwaizumi, T. Kudo and S. Kita, *Inorg. Chem.,* 1986, **25**, 1546-1550). This is consistent with the ~14 G (~39 MHz) splitting that is resolved near g = 2 in the spectra for compounds **3** and **5**. We found that no combination, or permutation, of these two tensors alone produced a feature at 3180 G. Only the combination of one ^{14}N with $[A_{||}, A_{\perp}]$ = [20, 40] and two with $[A_{||}, A_{\perp}]$ = [40, 20], with a fourth ^{14}N with a 40 MHz isotropic coupling, satisfactorily reproduced the $g_{||}$ region of the spectrum, and specifically the feature at 3180 G. Any other combination that produced a feature near that position also produced poorly resolved features to lower field that are not reflected in the spectra.

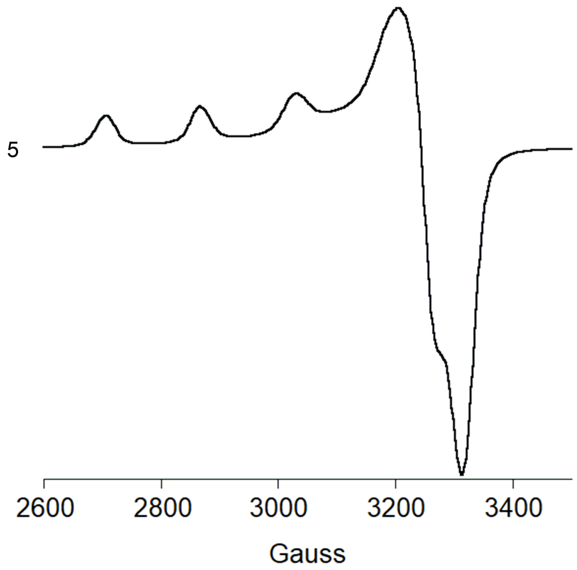

Figure S2. EPR spectrum of **6** in CH_3CN:toluene (1:1) at 12 K**.** Parameters: $g_{||}$= 2.27, $g_{\perp}$ = 2.07, and $^{63,65}Cu$ couplings of [$A_{||}$, $A_{\perp}$] = [530, 116] MHz.

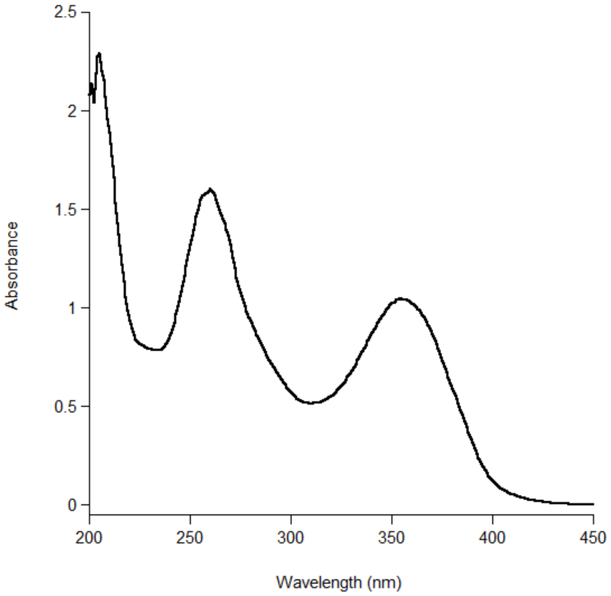

Figure S3. Absorption spectrum of **3** (6.0×10^{-5} M) in CH_3CN.

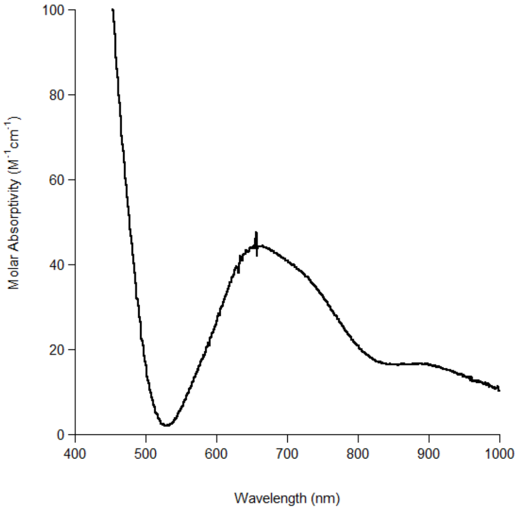

Figure S4. UV-Vis spectrum of the *d-d* region of **3** in CH_3CN.

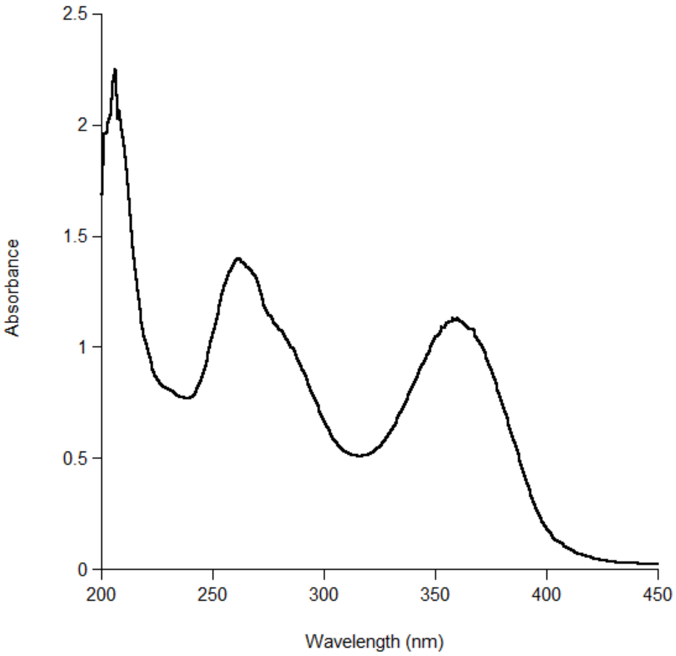

Figure S5. Absorption spectrum of **4** (6.2 x 10^{-5} M) in CH$_3$CN.

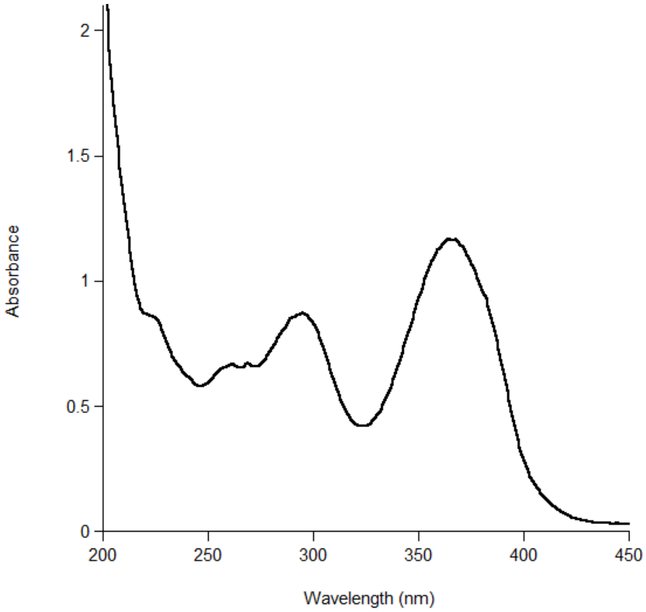

Figure S6. Absorption spectrum of **5** (4.0 x 10^{-5} M) in CH$_3$CN.

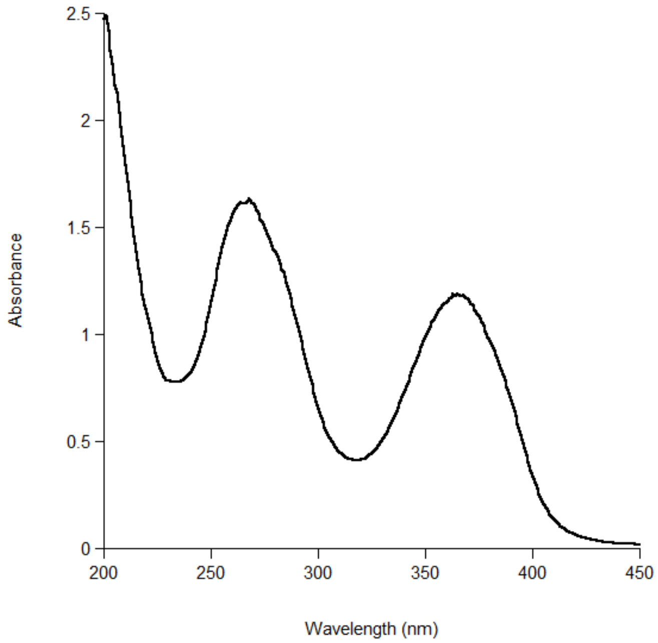

Figure S7. Absorption spectrum of **6** (6.12×10^{-5} M) in CH_3CN.

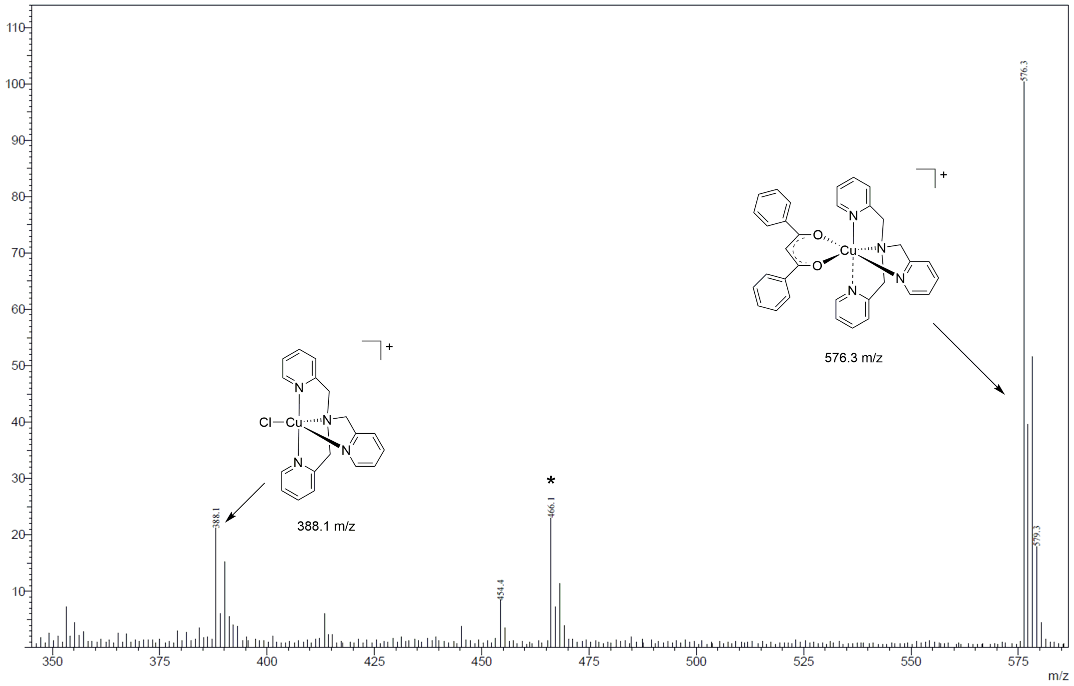

Figure S8. ESI-MS of isolated **3** in CH_3CN. The ***** near the isotope cluster *m/z* 466.1 represents an adduct of trifluoro acetic acid (TFA) with $[TPACu]^{2+}$, which is due to contamination in the mass spectrometer.

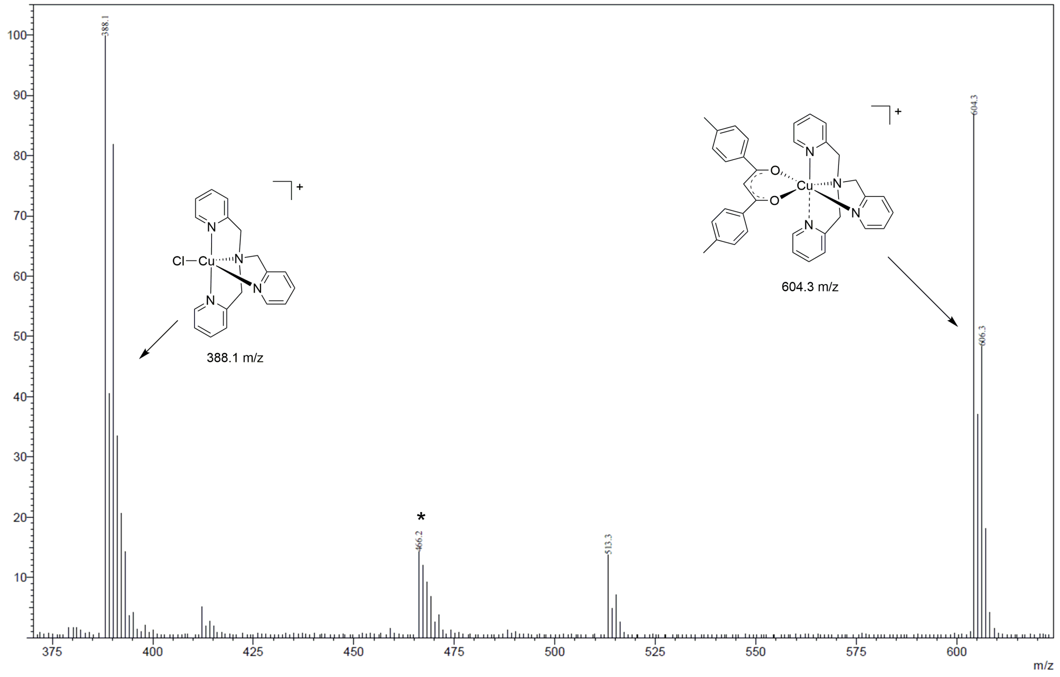

Figure S9. ESI-MS of isolated **4** in CH_3CN. The ***** near the isotope cluster *m/z* 466.2 represents an adduct of trifluoro acetic acid (TFA) with $[TPACu]^{2+}$, which is due to contamination in the mass spectrometer.

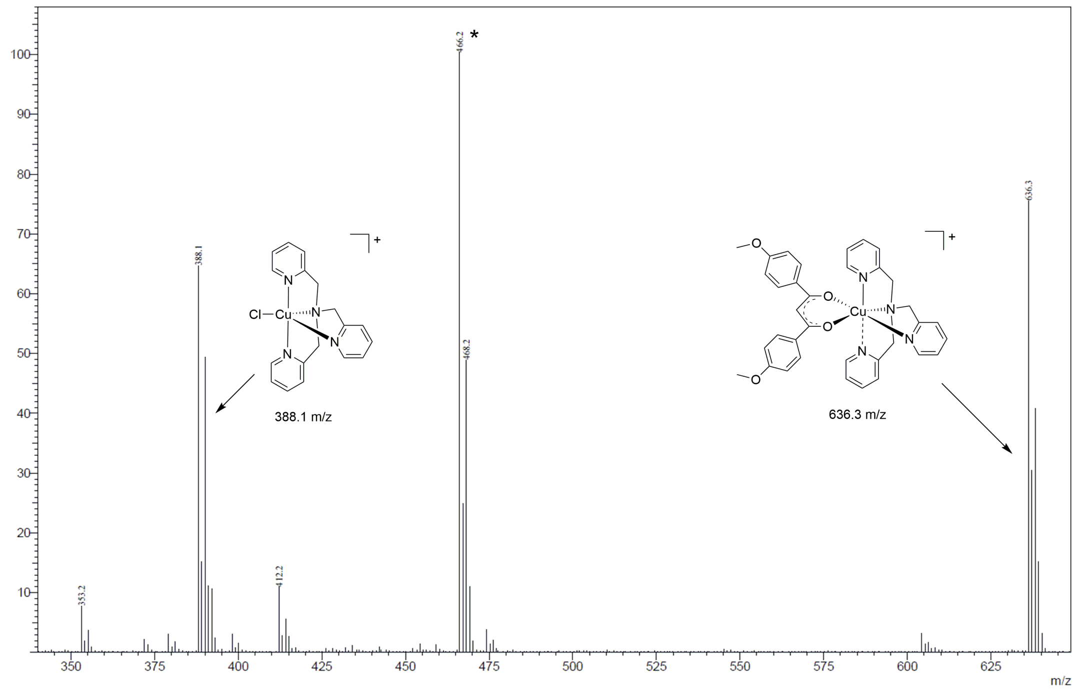

Figure S10. ESI-MS of **5** in CH_3CN. The * near the isotope cluster *m/z* 466.2 represents an adduct of trifluoro acetic acid (TFA) with $[TPACu]^{2+}$, which due to contamination in the mass spectrometer.

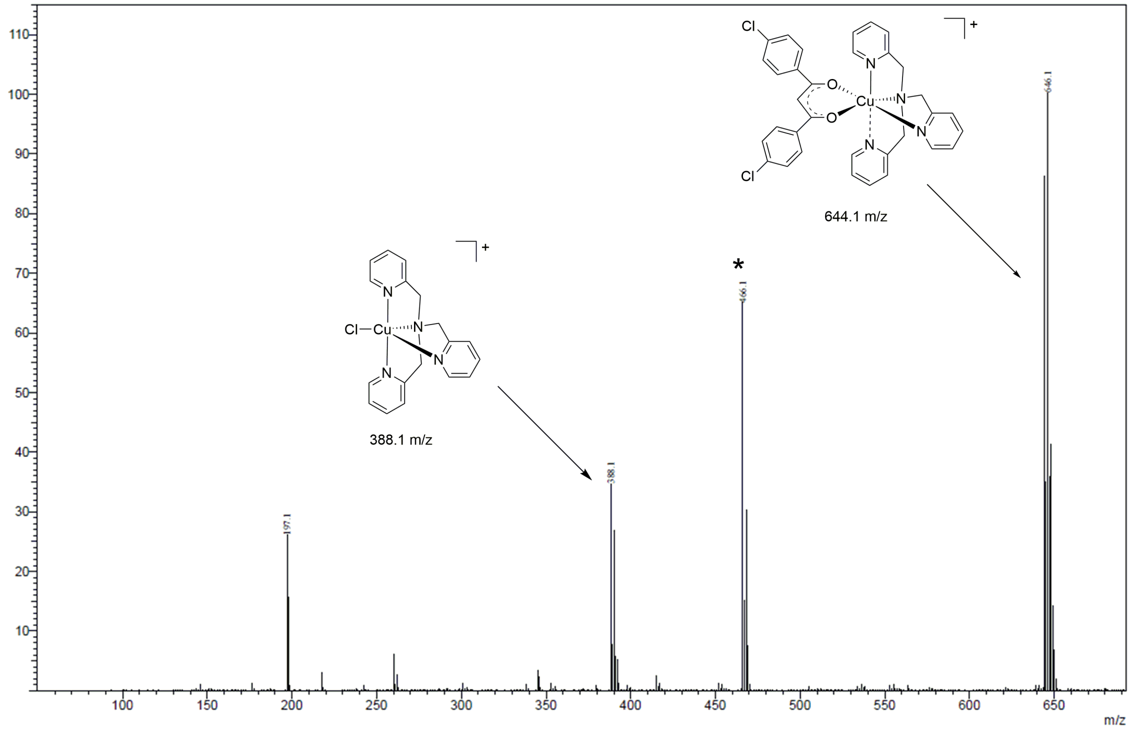

Figure S11. ESI-MS of **6** in CH_3CN. The * near the isotope cluster *m/z* 466.1 represents an adduct of trifluoro acetic acid (TFA) with $[TPACu]^{2+}$, which is due to contamination in the mass spectrometer.

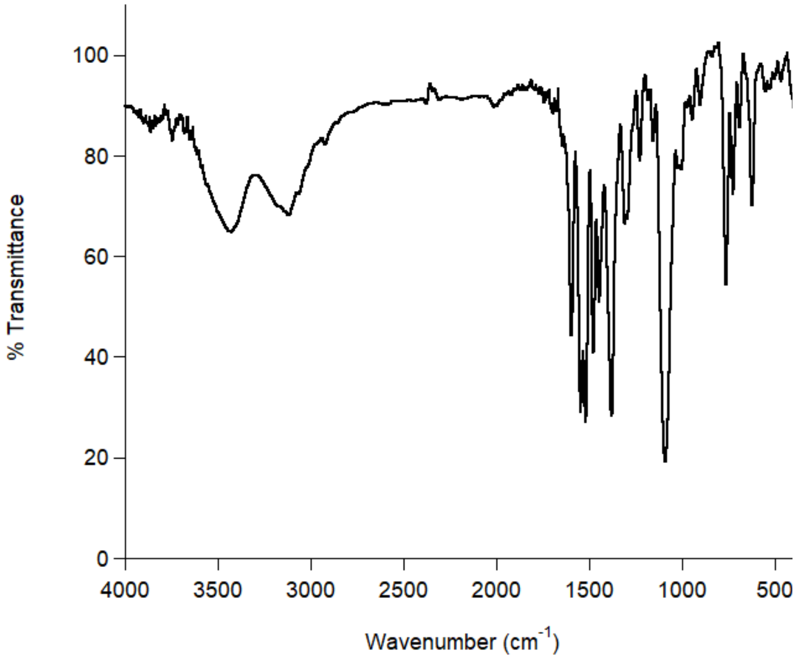

Figure S12. IR spectrum of **3** (KBr pellet).

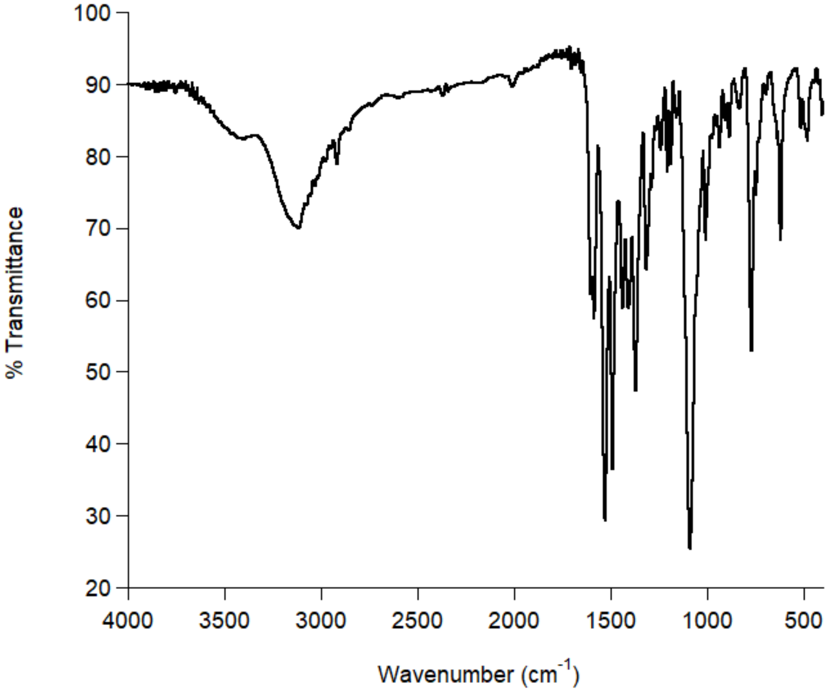

Figure S13. IR spectrum of **4** (KBr pellet).

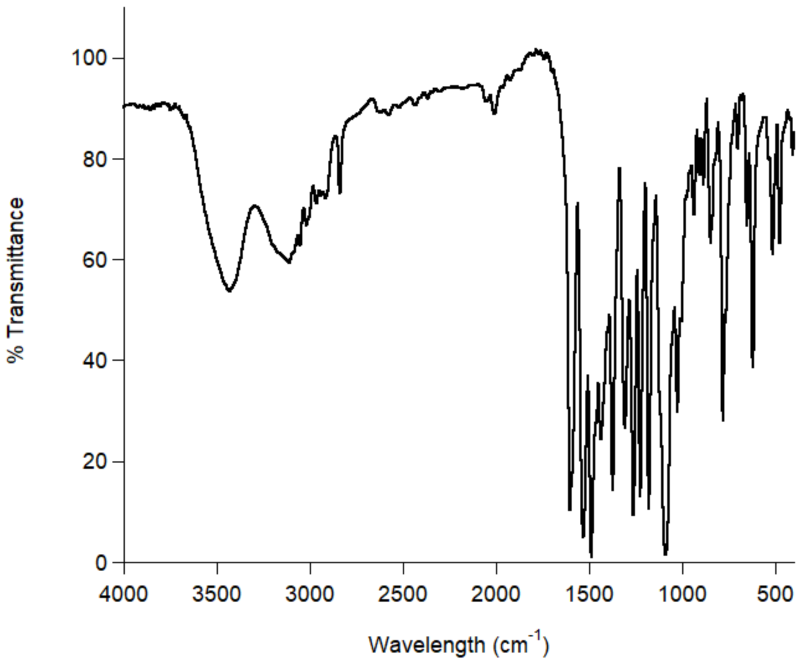

Figure S14. IR spectrum of **5** (KBr pellet).

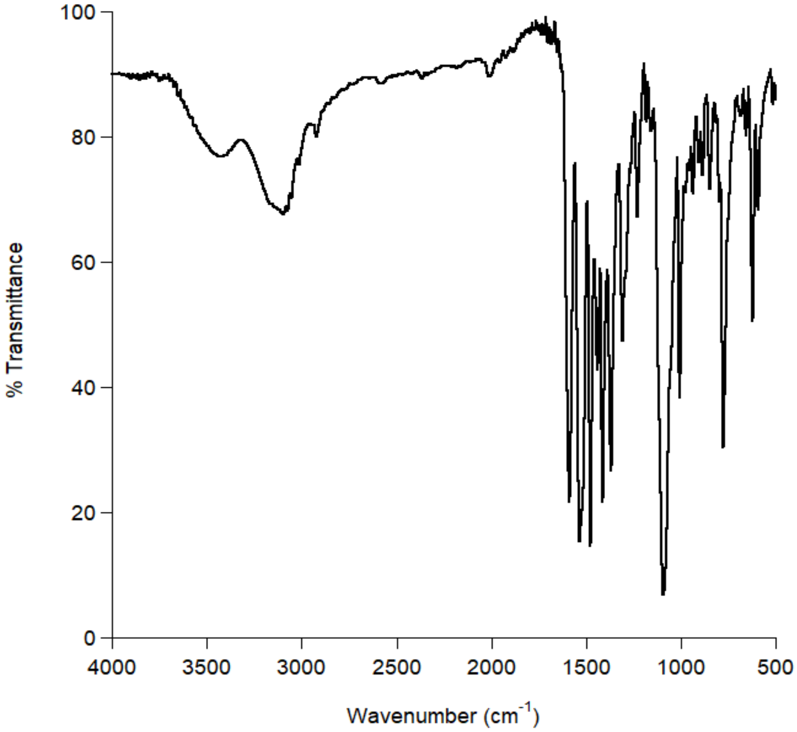

Figure S15. IR spectrum of **6** (KBr pellet).

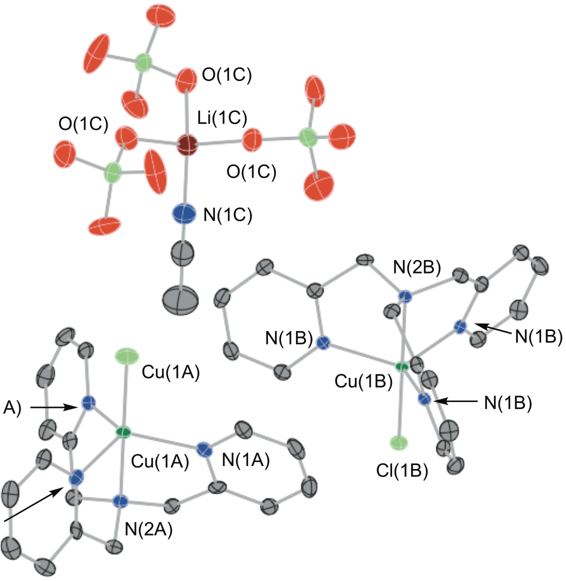

Figure S16. Representations of the cationic and anionic portions of the X-ray structure of **11**. Ellipsoids are plotted at the 50% probability level.

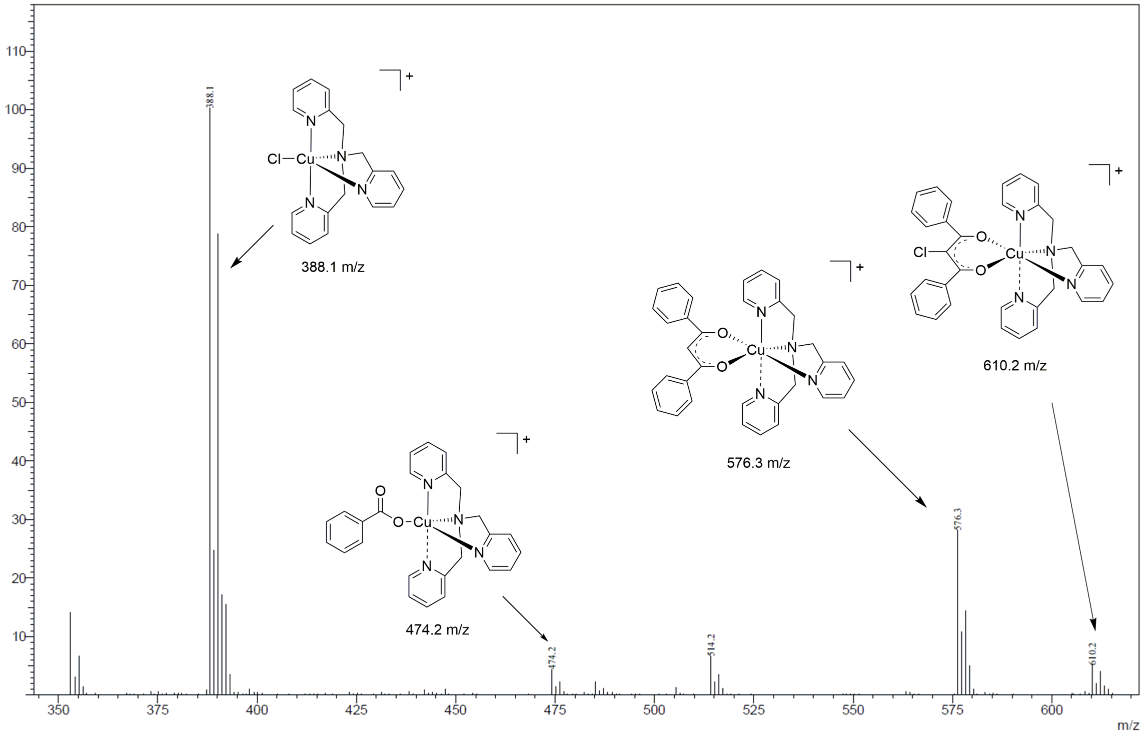

Figure S17. ESI-MS (CH_3CN)of the reaction mixture for the attempted preparation of **7**.

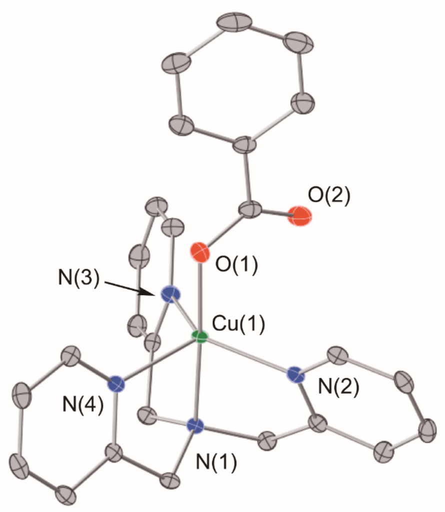

Figure S18. Representation of the cationic portion of the X-ray structure of **12**. Ellipsoids are plotted at the 50% probability level.

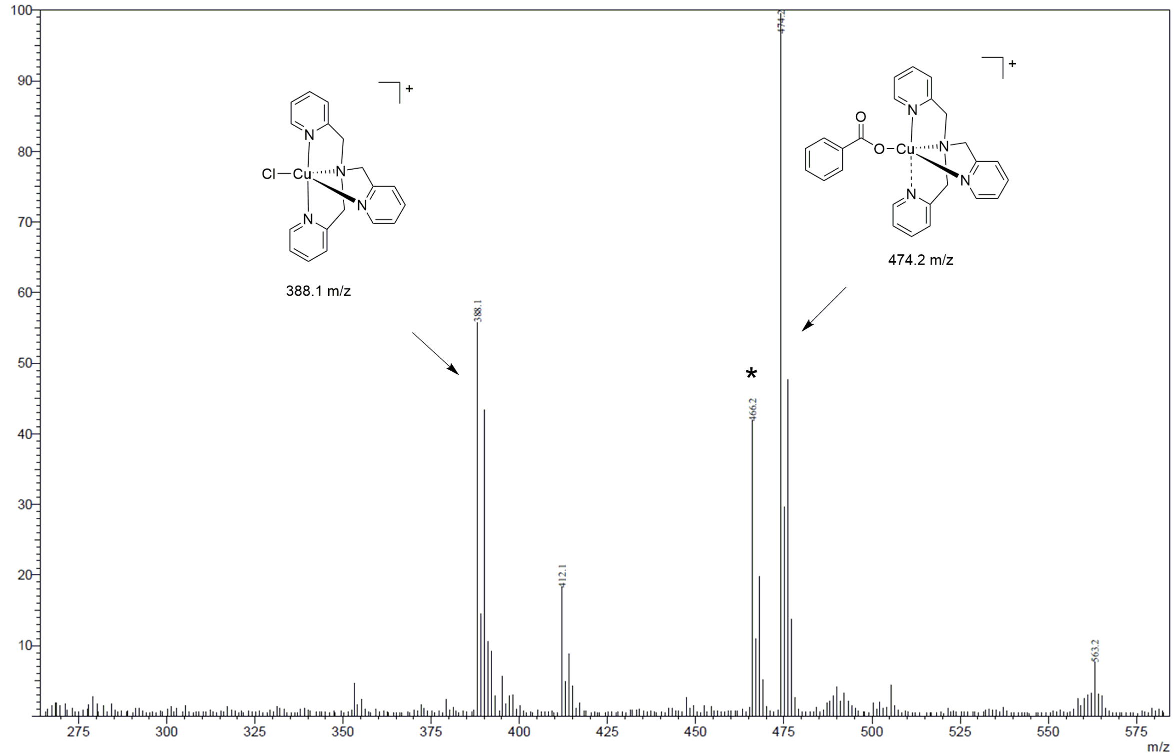

Figure S19. ESI-MS of **12** in CH_3CN. The ***** near the isotope cluster *m/z* 466.2 represents an adduct of trifluoro acetic acid (TFA) with $[TPACu]^{2+}$, which is due to contamination in the mass spectrometer.

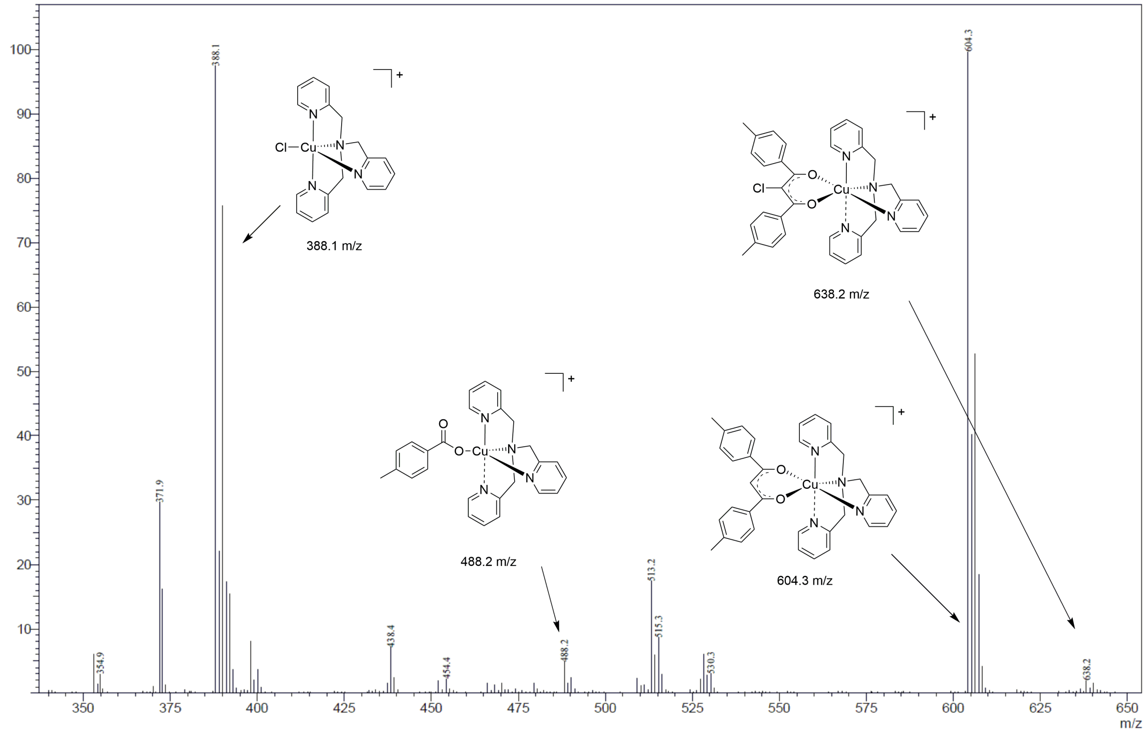

Figure S20. ESI-MS (CH_3CN) of the reaction mixture for the attempted preparation of **8.**

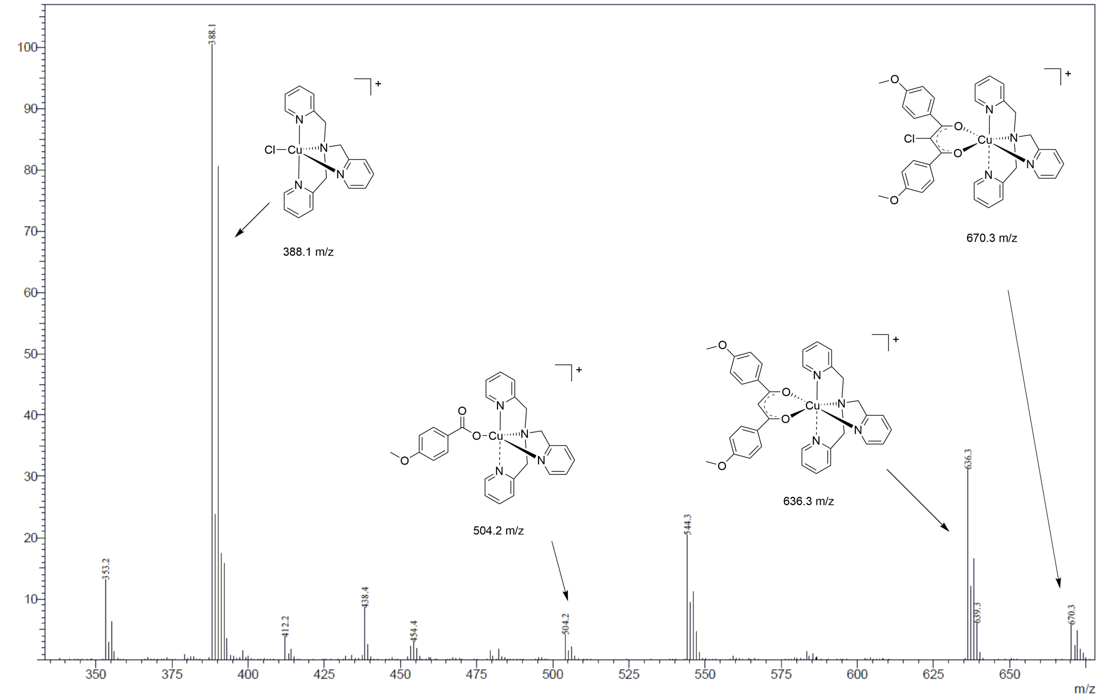

Figure S21. ESI-MS (CH_3CN) of the reaction mixture for the attempted preparation of **9.**

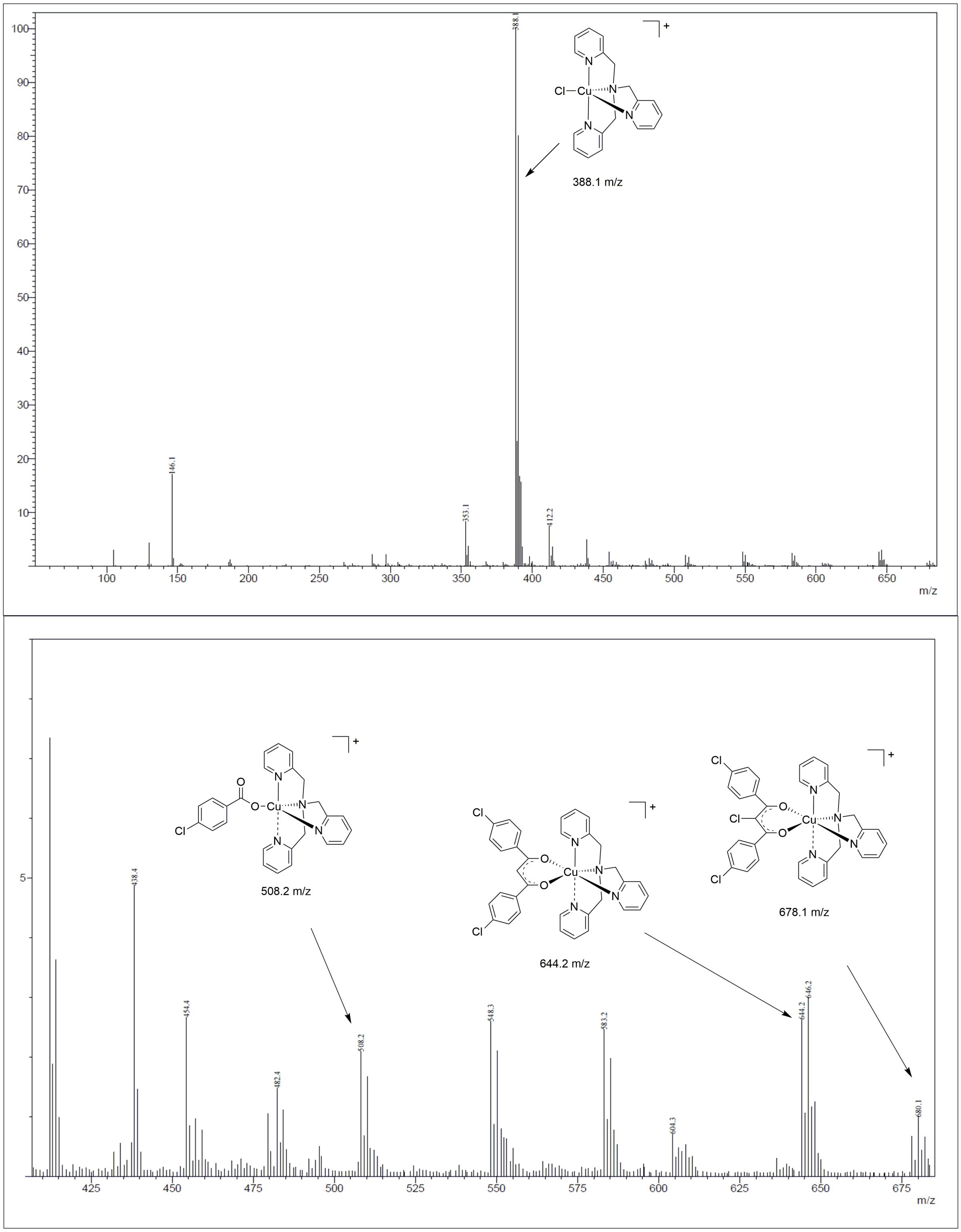

Figure S22. ESI-MS (CH_3CN) of the reaction mixture for the attempted preparation of **10.**

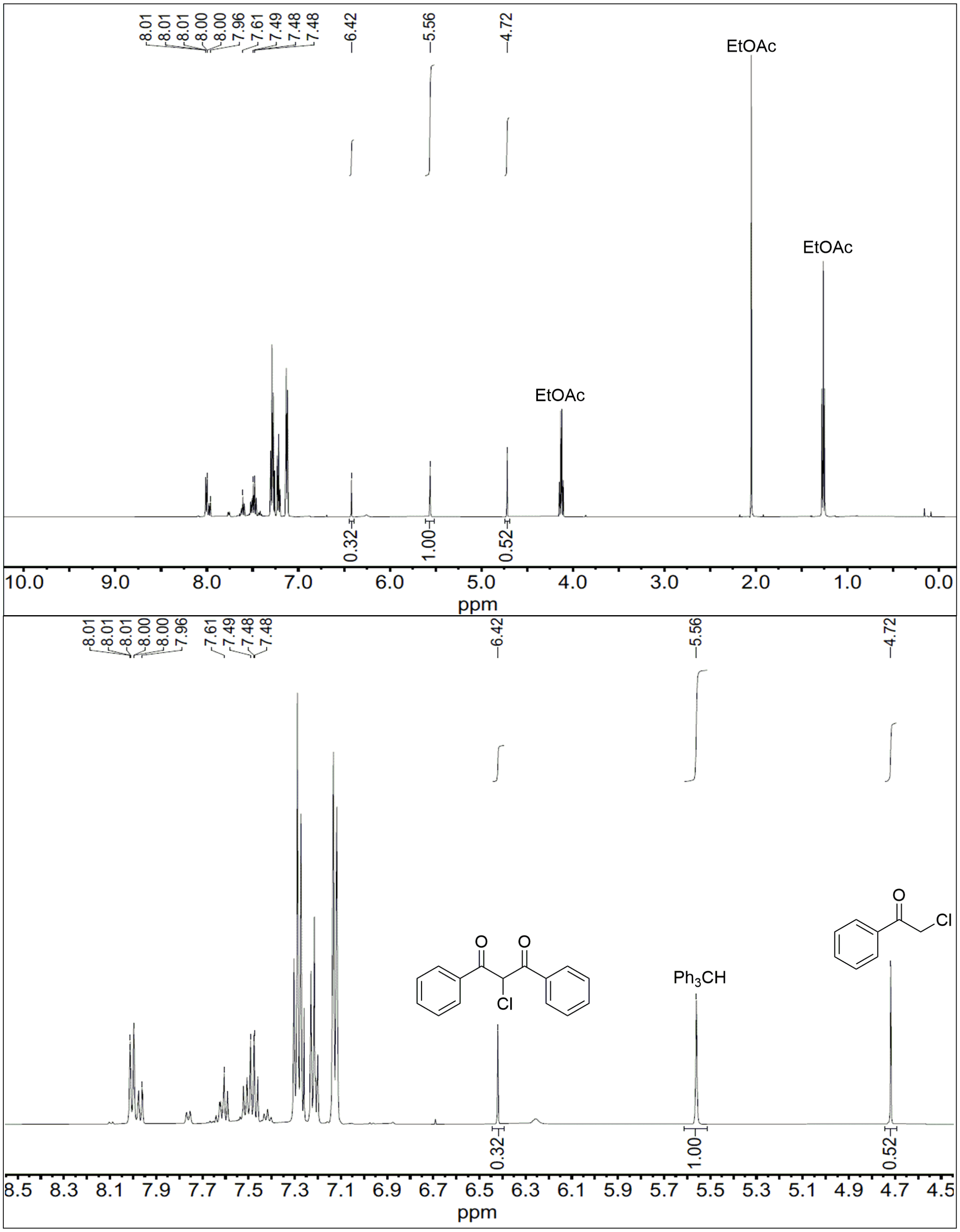

Figure S23. ^{1}H NMR (CD_3CN) of the organic recovery from the reaction mixture of **7**. Ph_3CH is present as an internal standard.

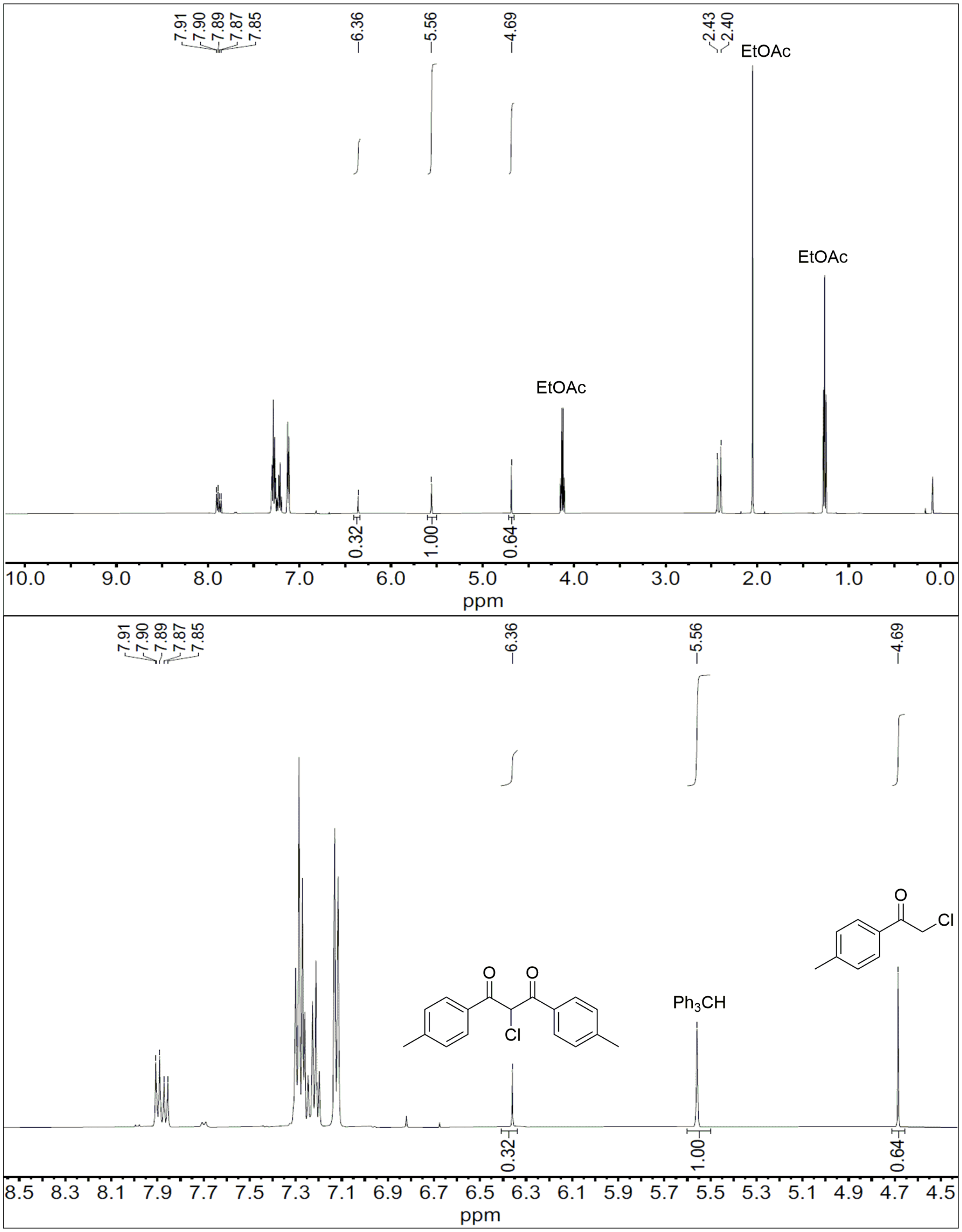

Figure S24. ^{1}H NMR (CD_3CN) of the organic recovery from the reaction mixture of **8**. Ph_3CH is present as an internal standard.

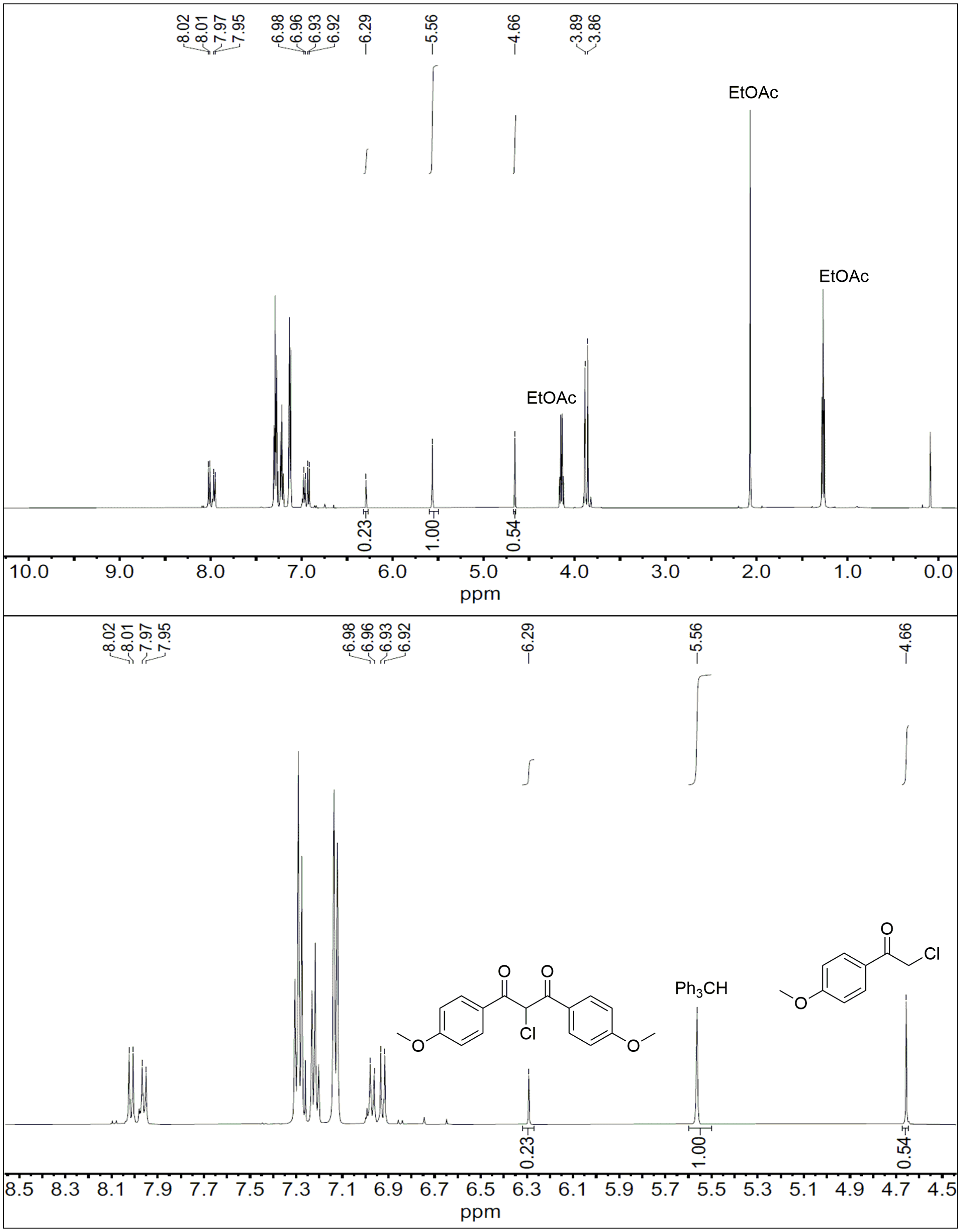

Figure S25. ^{1}H NMR (CD_3CN) of the organic recovery from the reaction mixture of **9**. Ph_3CH is present as an internal standard.

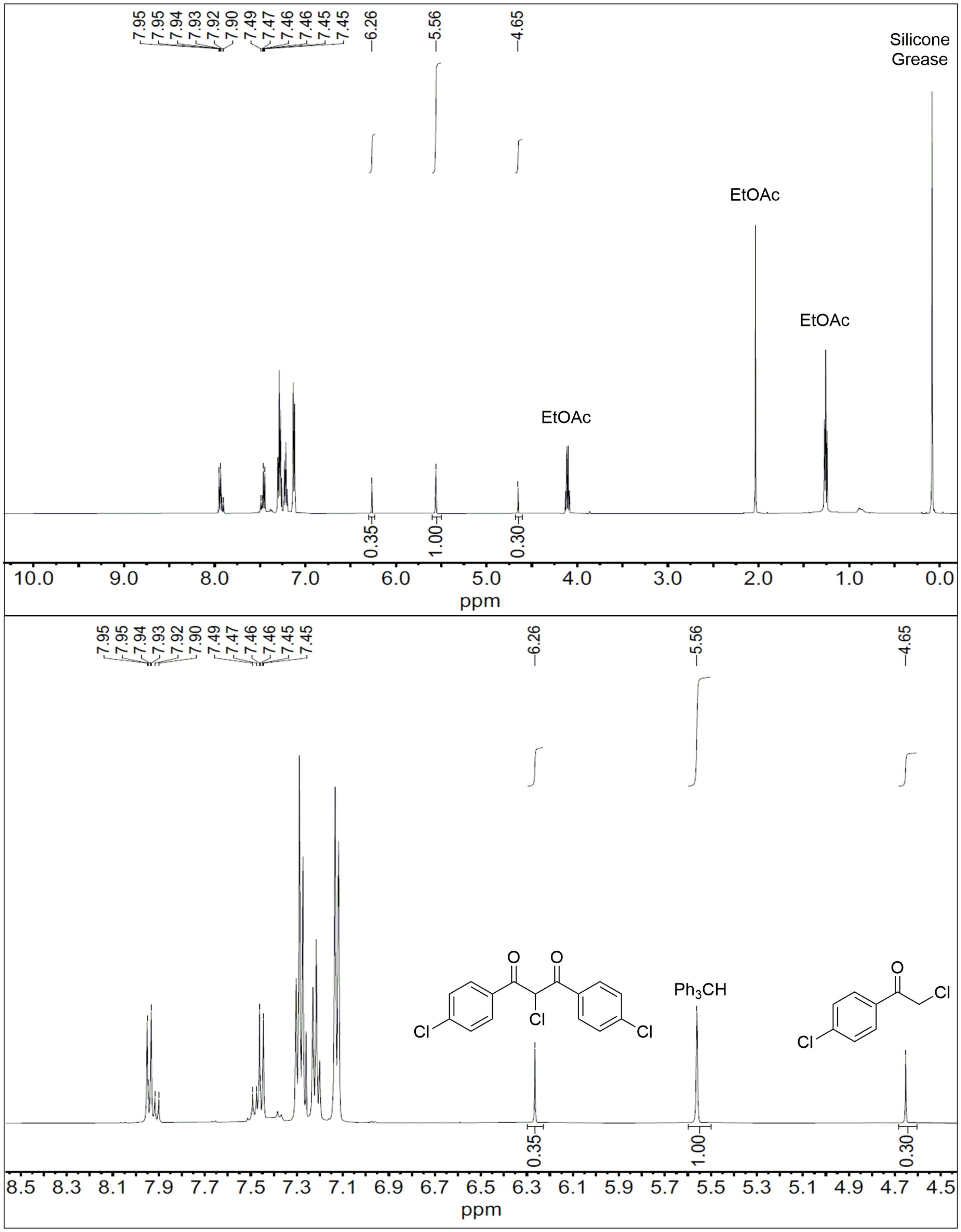

Figure S26. ^{1}H NMR (CD_3CN) of the organic recovery from the reaction mixture of **10**. Ph_3CH is present as an internal standard.

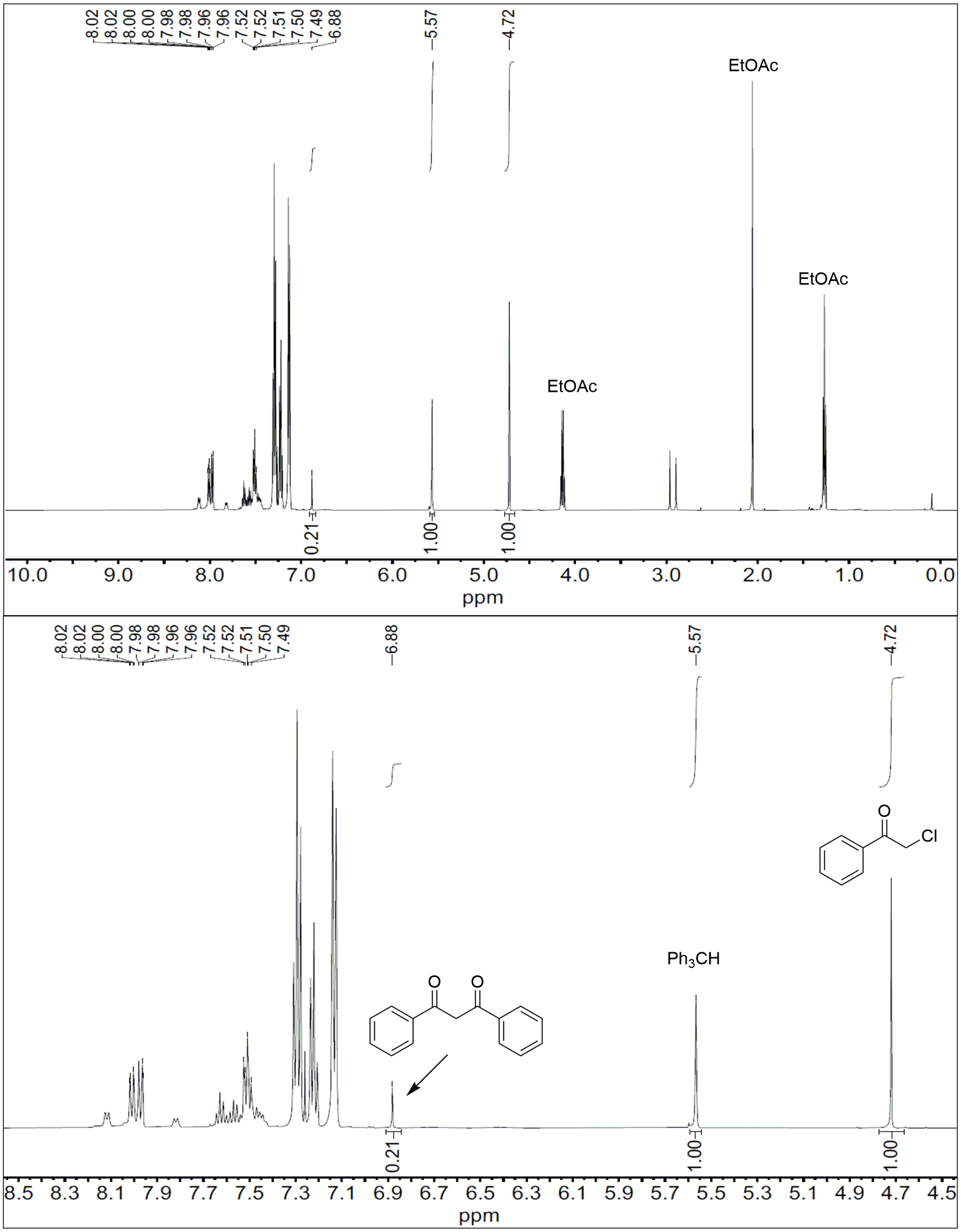

Figure 27. ^{1}H NMR (CD_3CN) of the free organic products from the reaction mixture of **7** with excess H_2O (200 eq). Ph_3CH is present as an internal standard.

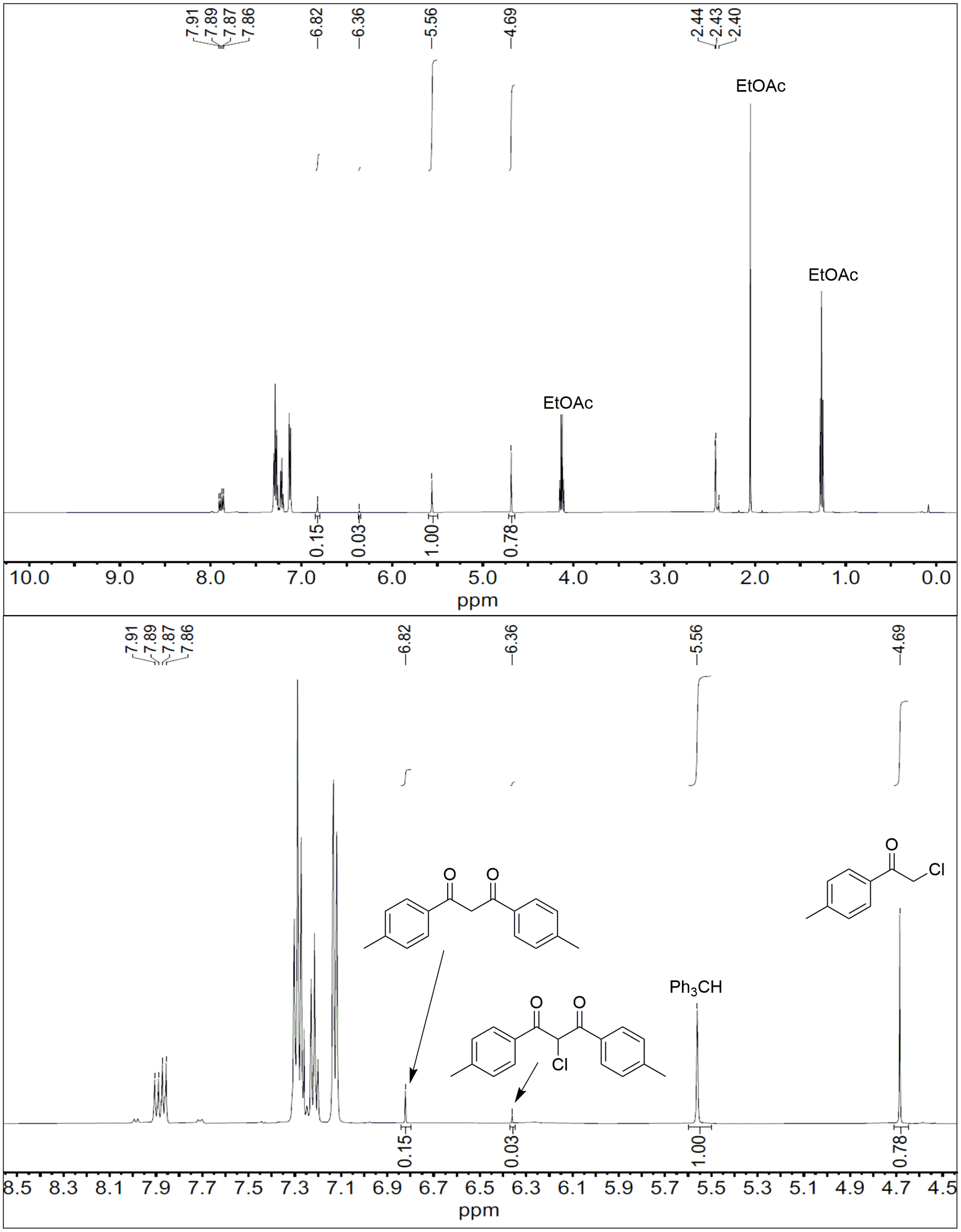

Figure 28. ^{1}H NMR (CD_3CN) of the free organic products from the reaction mixture of **8** with excess H_2O (200 eq). Ph_3CH is present as an internal standard.

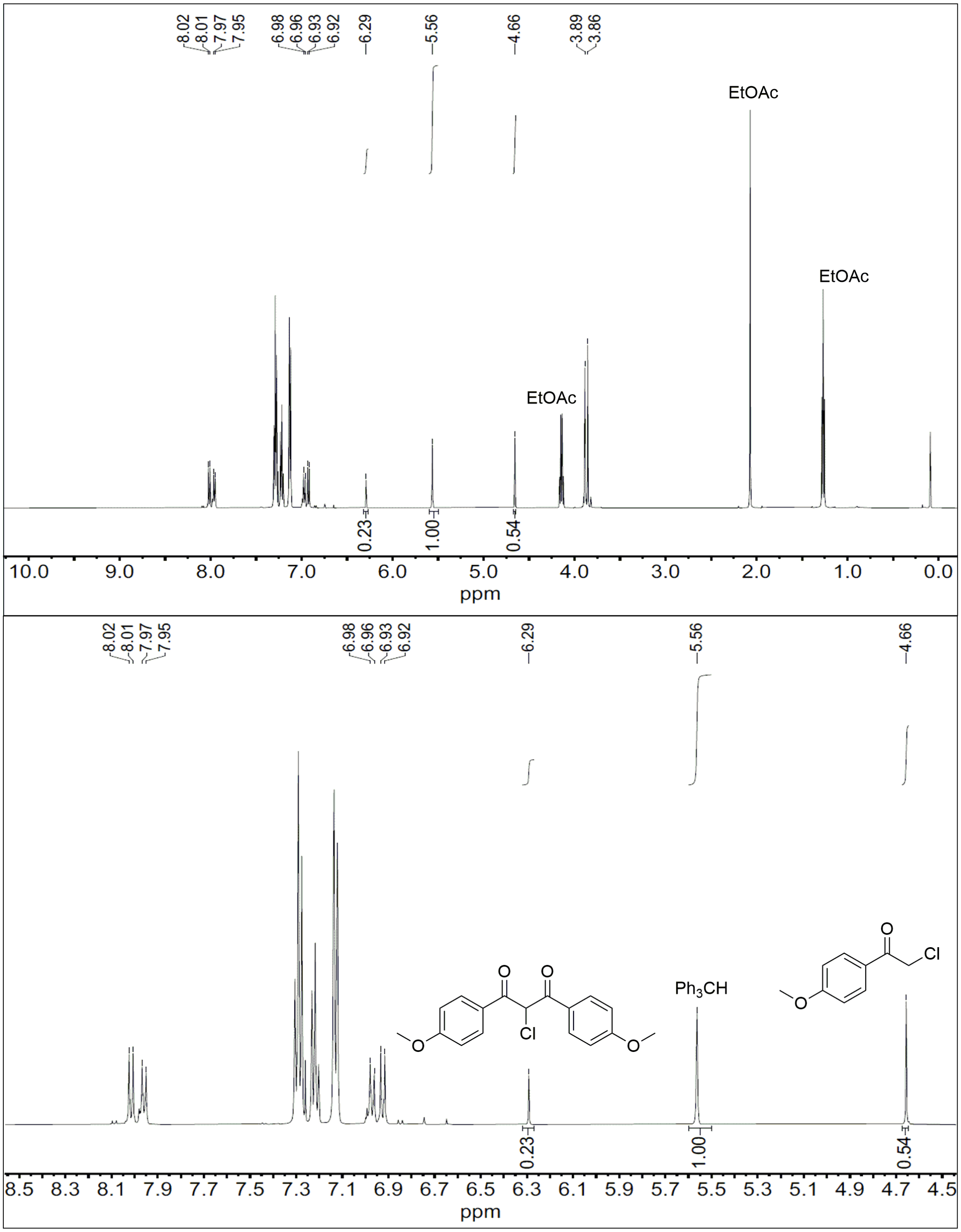

Figure S29. ^{1}H NMR (CD_3CN) of the free organic products from the reaction mixture of **9** with excess H_2O (200 eq). Ph_3CH is present as an internal standard.

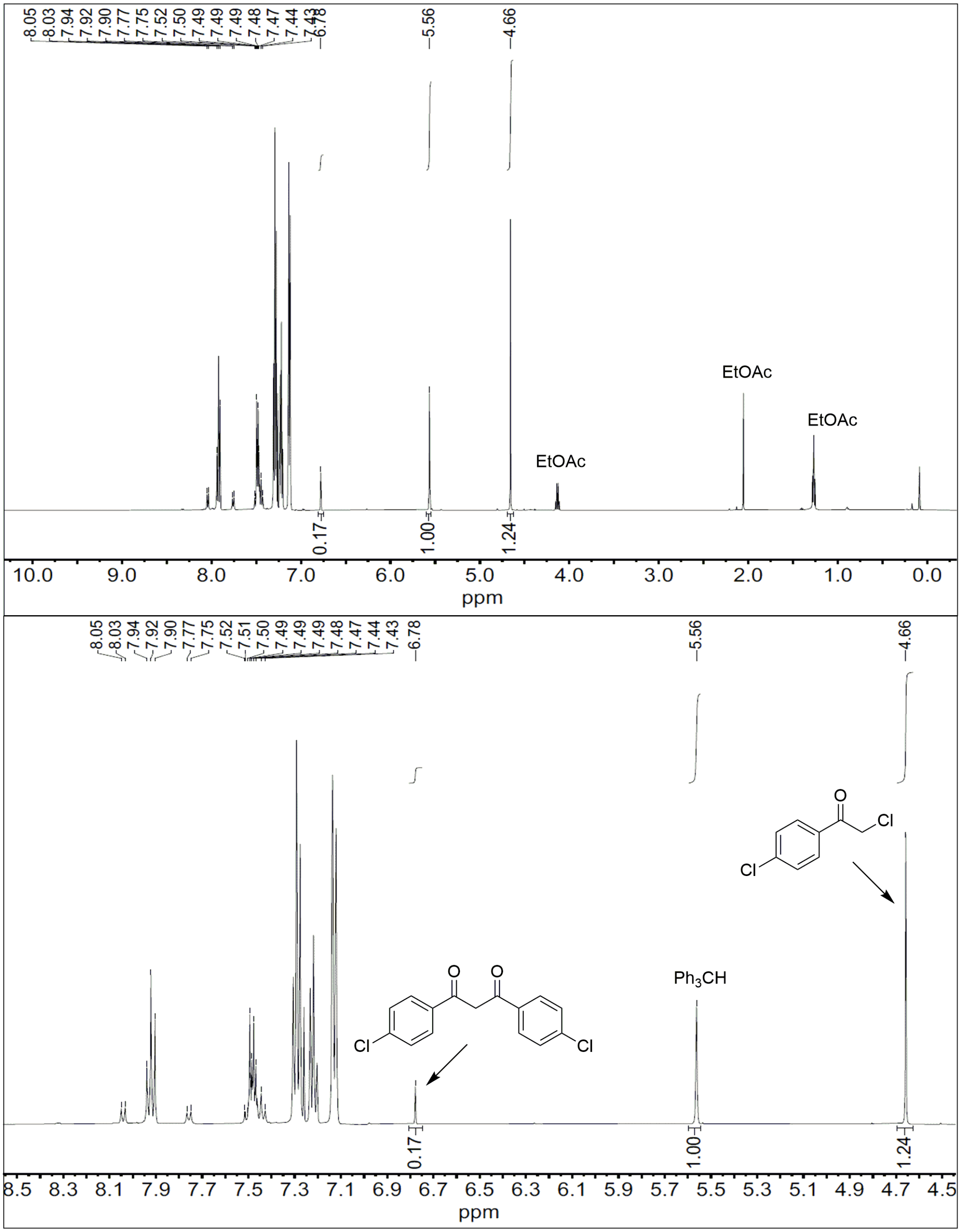

Figure S30. ^{1}H NMR (CD_3CN) of the free organic products from the reaction mixture of **10** with excess H_2O (200 eq). Ph_3CH is present as an internal standard.

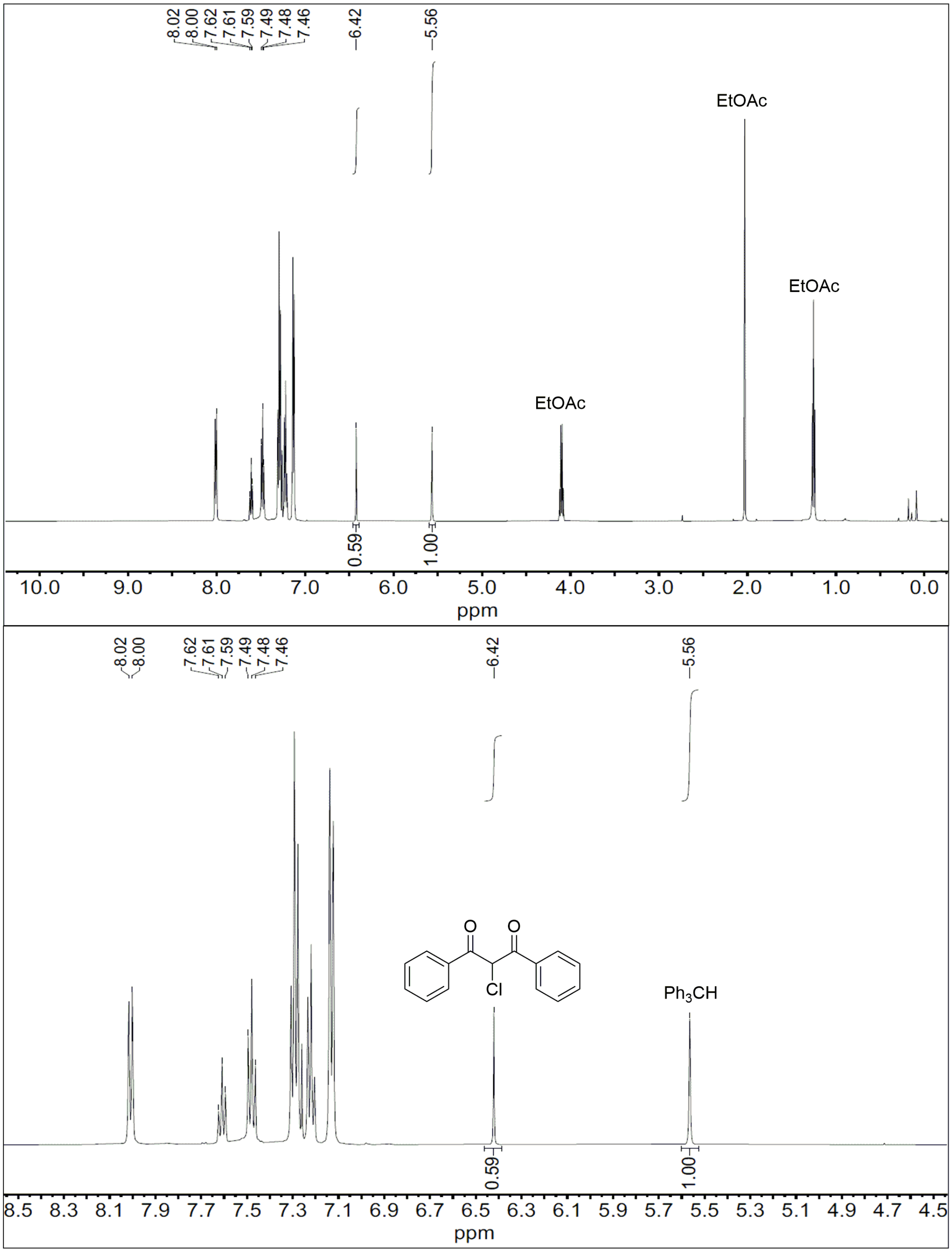

Figure S31. ^{1}H NMR (CD_3CN) of the organic recovery from the reaction mixture of $[(TPA)Cu(CH_3CN)](ClO_4)_2$, LiHMDS, and 2-chloro-1,3-phenylpropane-1,3-dione. Ph_3CH is present as an internal standard.

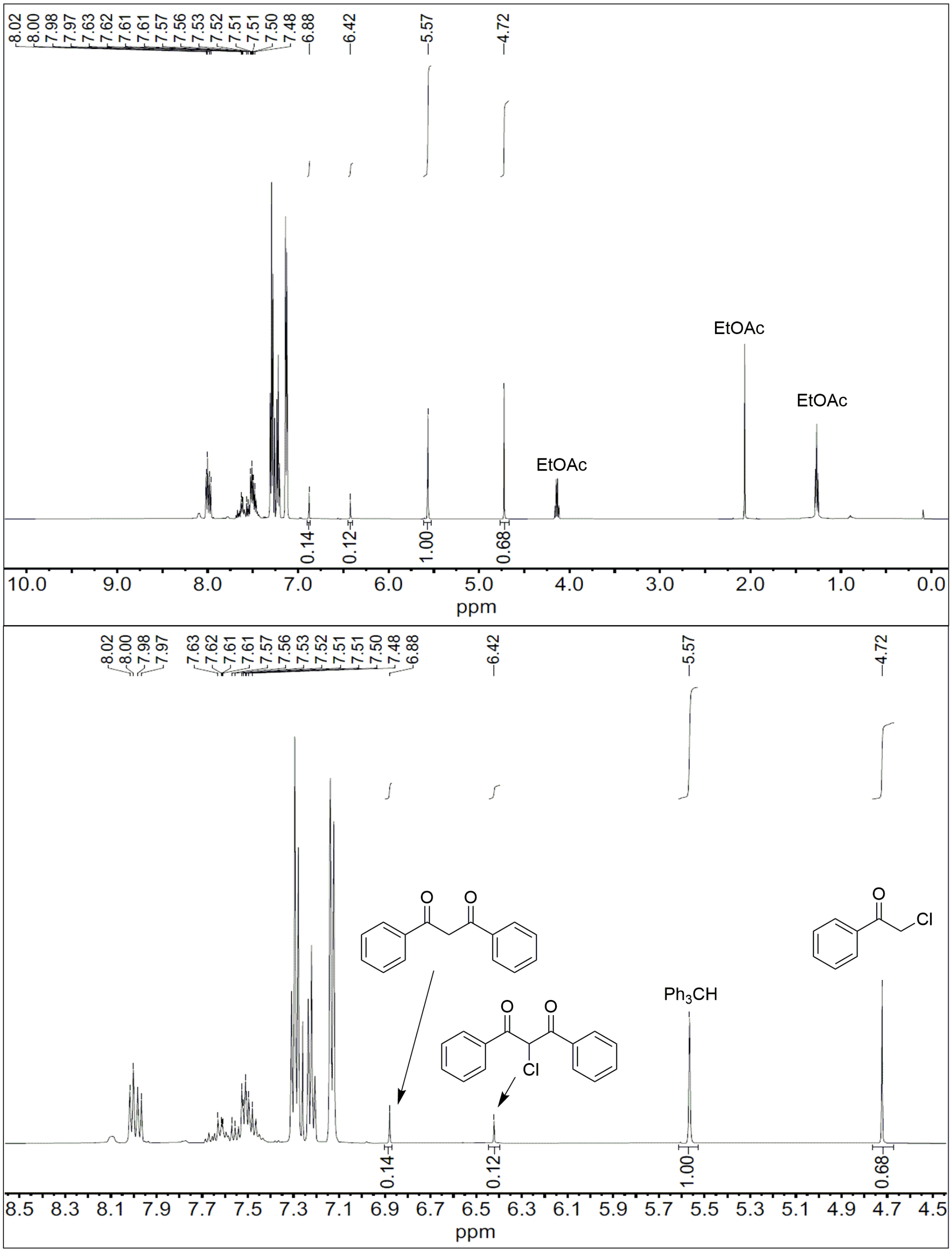

Figure S32. ^{1}H NMR (CD_3CN) of the organic recovery from the reaction mixture of $[(TPA)Cu(CH_3CN)](ClO_4)_2$, LiHMDS, 2-chloro-1,3-phenylpropane-1,3-dione and excess H_2O (200 eq). Ph_3CH is present as an internal standard.

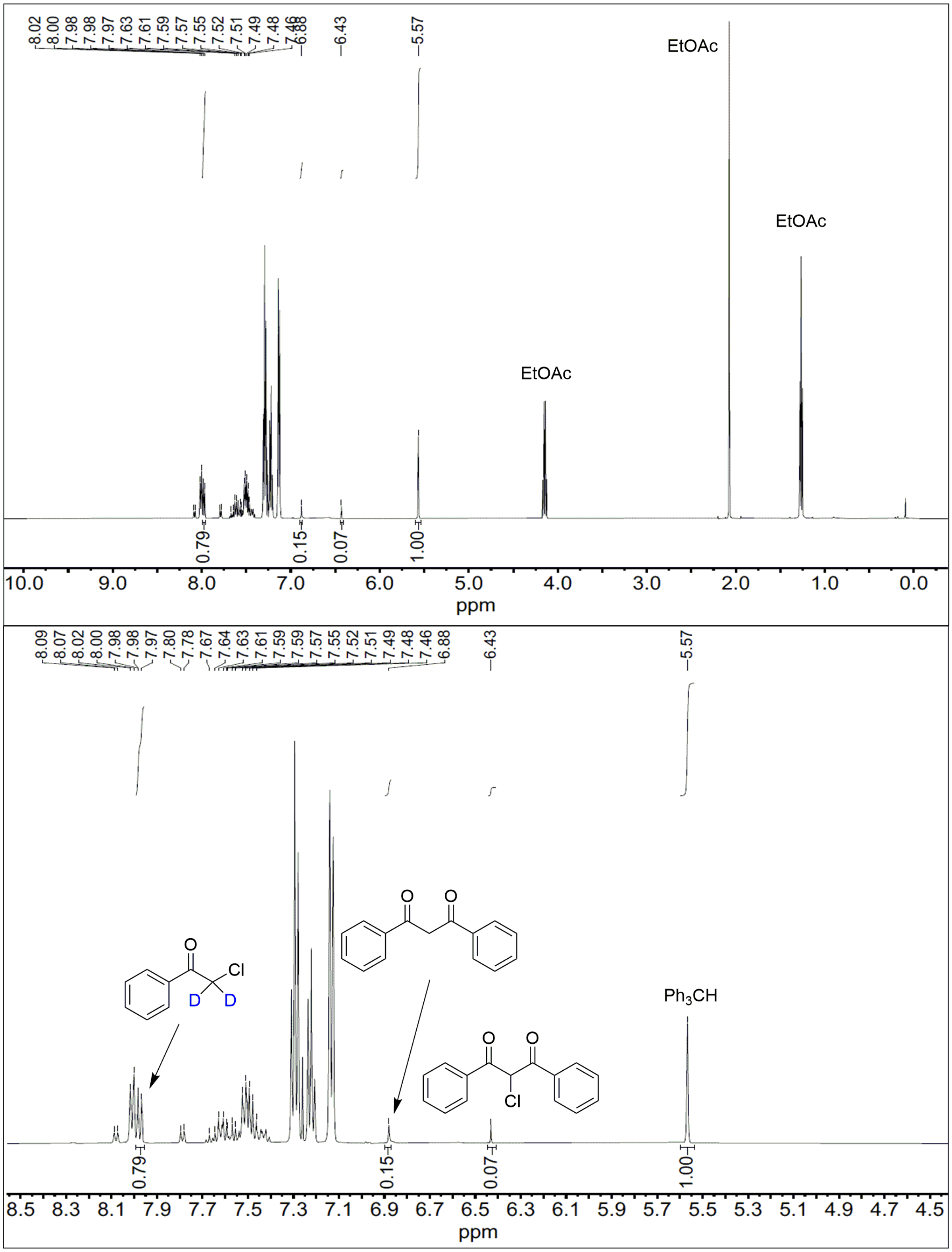

Figure S33. ^{1}H NMR (CD_3CN) of the organic recovery from the reaction mixture of $[(TPA)Cu(CH_3CN)](ClO_4)_2$, LiHMDS, 2-chloro-1,3-phenylpropane-1,3-dione and excess D_2O. Ph_3CH is present as an internal standard.

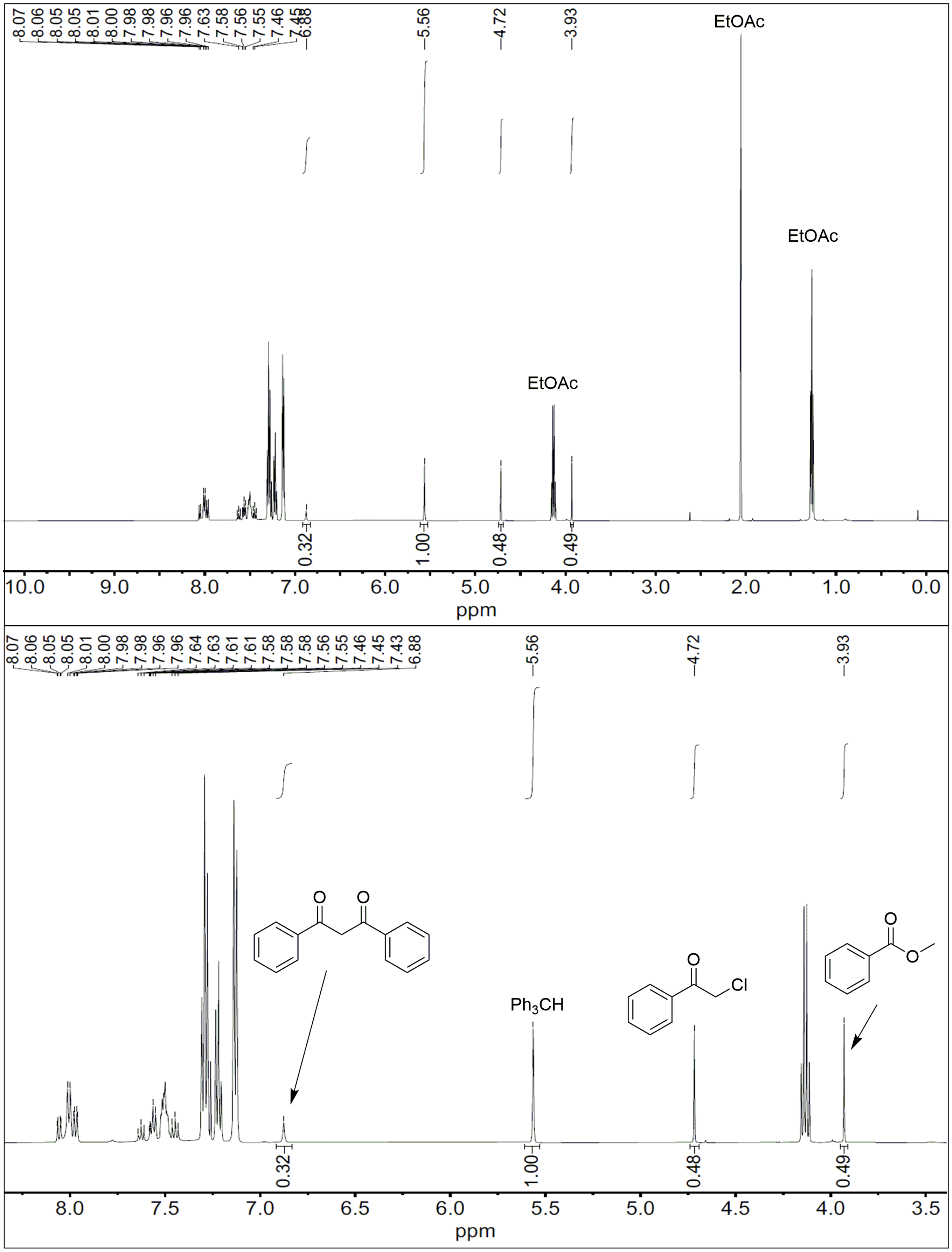

Figure S34. ^{1}H NMR (CD_3CN) of the organic recovery from the reaction mixture of $[(TPA)Cu(CH_3CN)](ClO_4)_2$, LiHMDS, 2-chloro-1,3-phenylpropane-1,3-dione and excess MeOH. Ph_3CH is present as an internal standard.

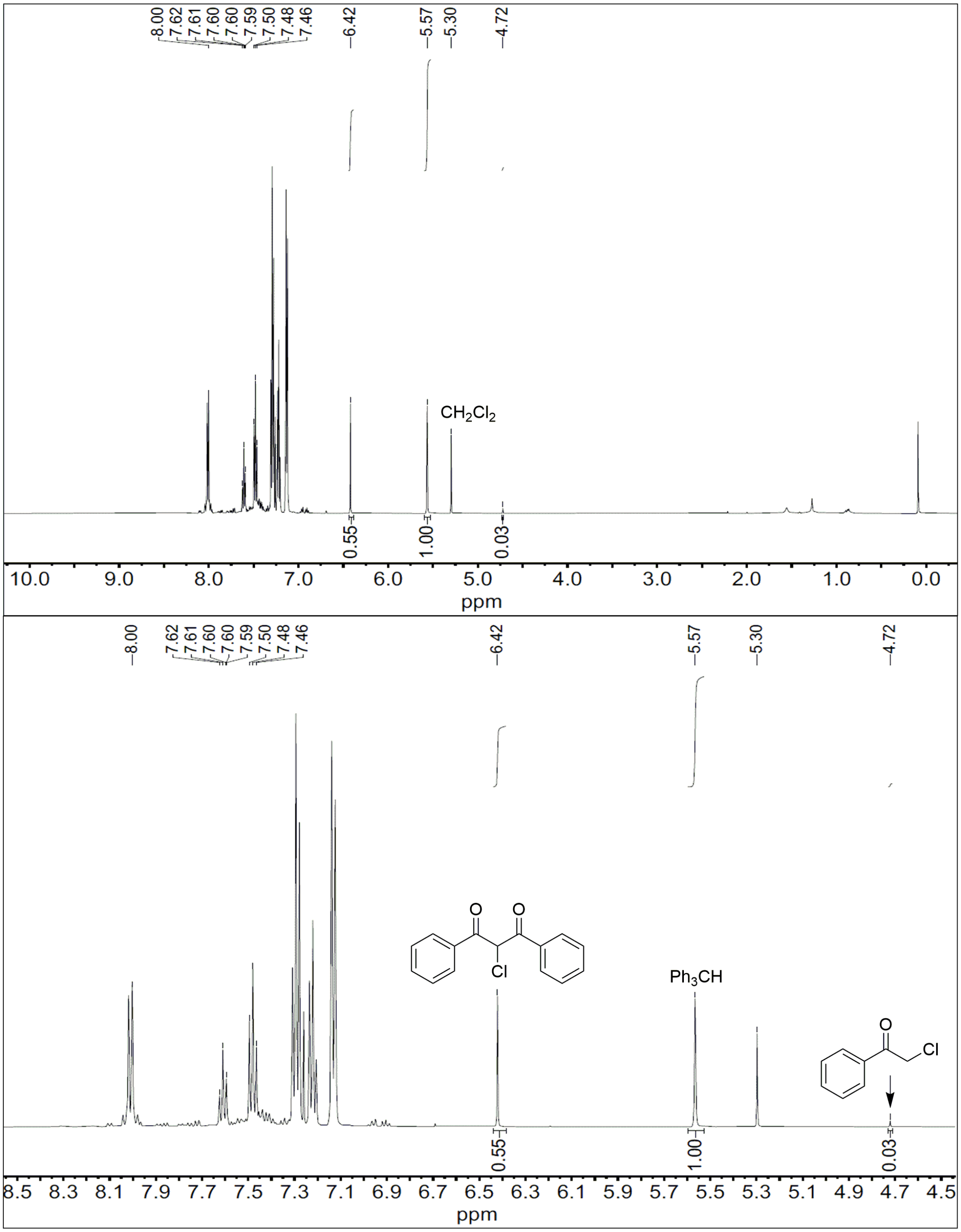

Figure S35. ^{1}H NMR (CD_3CN) of the organic recovery from the reaction mixture of $Cu(ClO_4)_2$•$6H_2O$, LiHMDS, and 2-chloro-1,3-phenylpropane-1,3-dione. Ph_3CH is present as an internal standard.

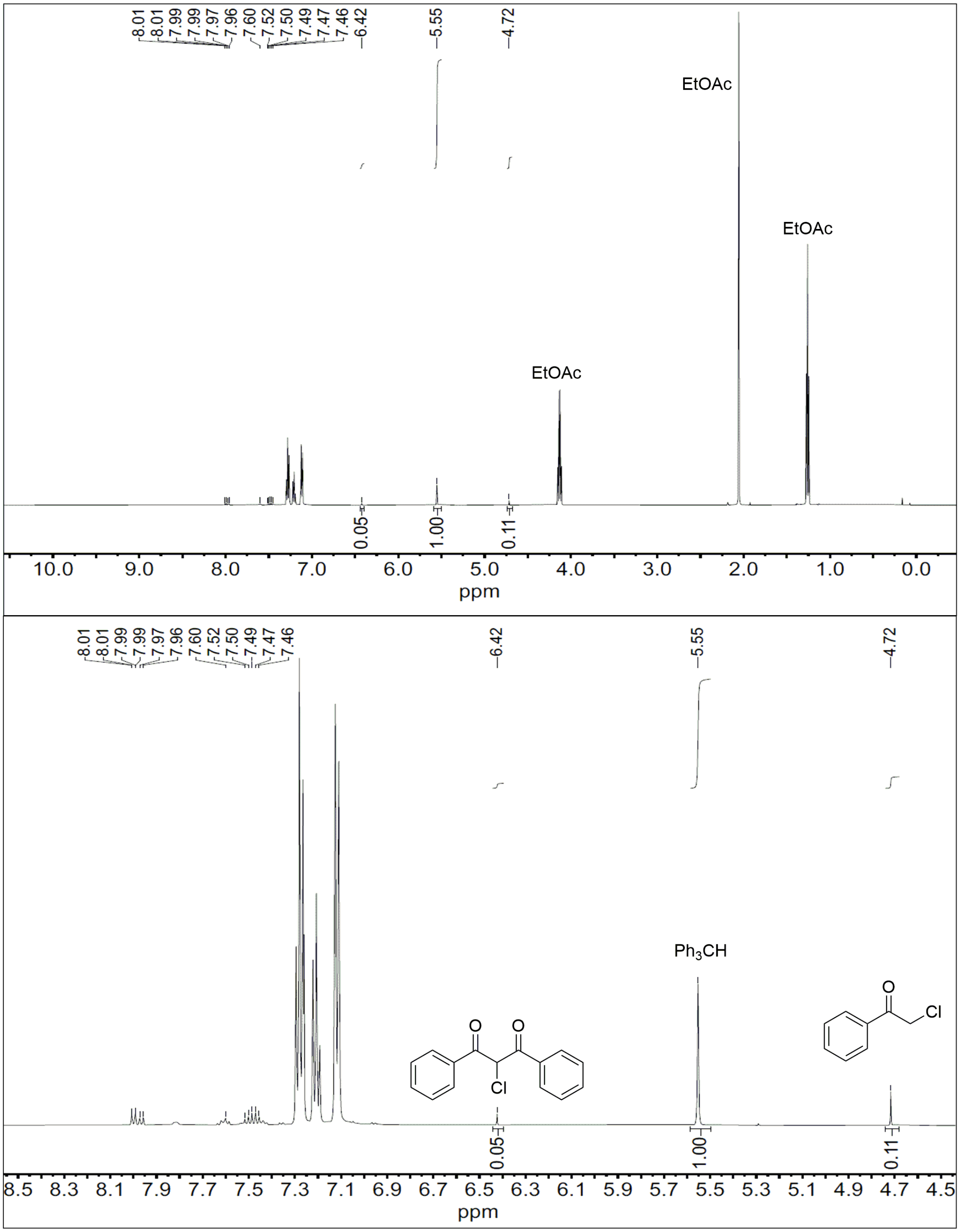

Figure S36. ^{1}H NMR (CD_3CN) of the organic recovery from the reaction mixture of in-situ generated **1**. Ph_3CH is present as an internal standard.

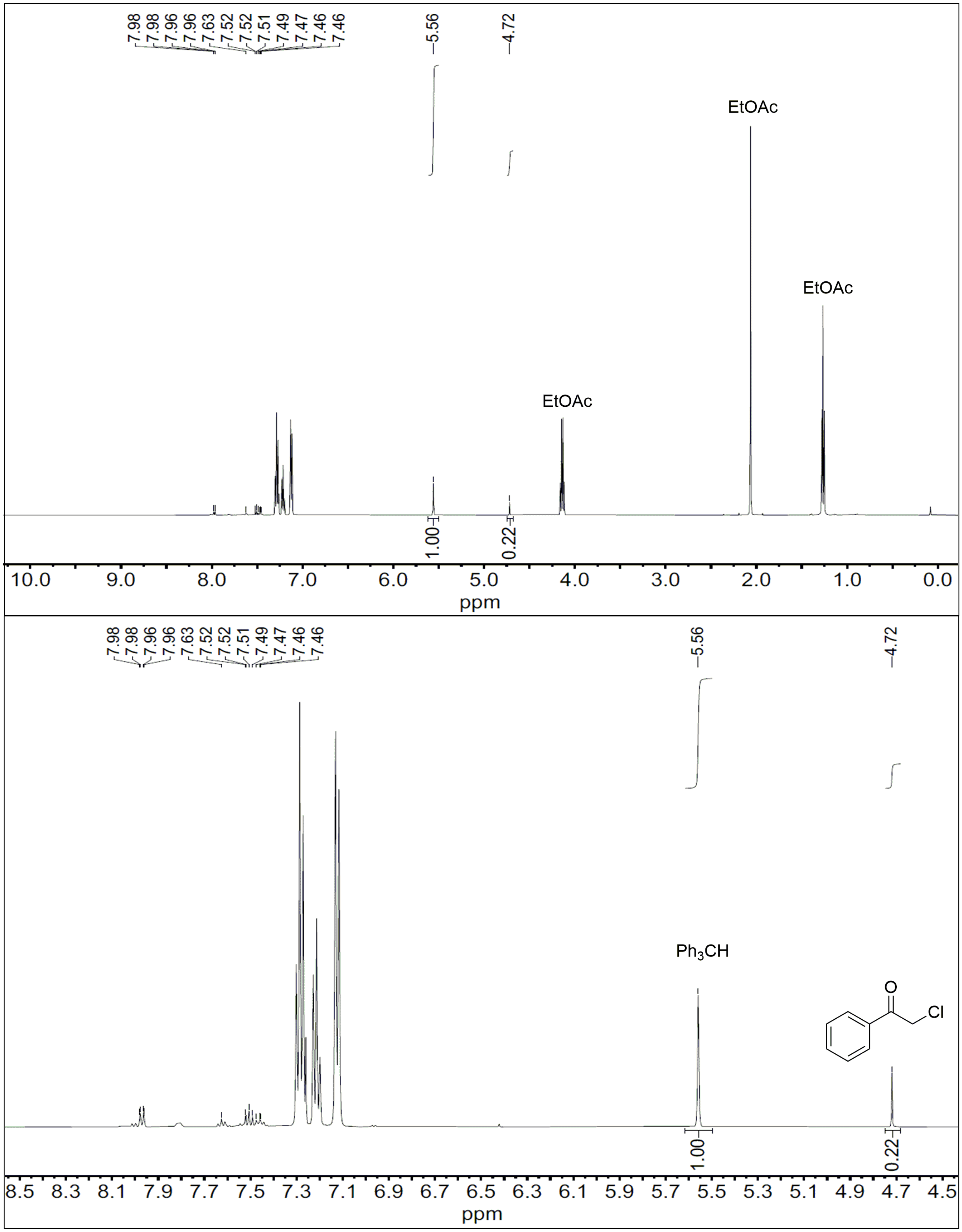

Figure S37. ^1H NMR (CD_3CN) of the organic recovery from the reaction mixture of in-situ generated **2**. Ph_3CH is present as an internal standard.

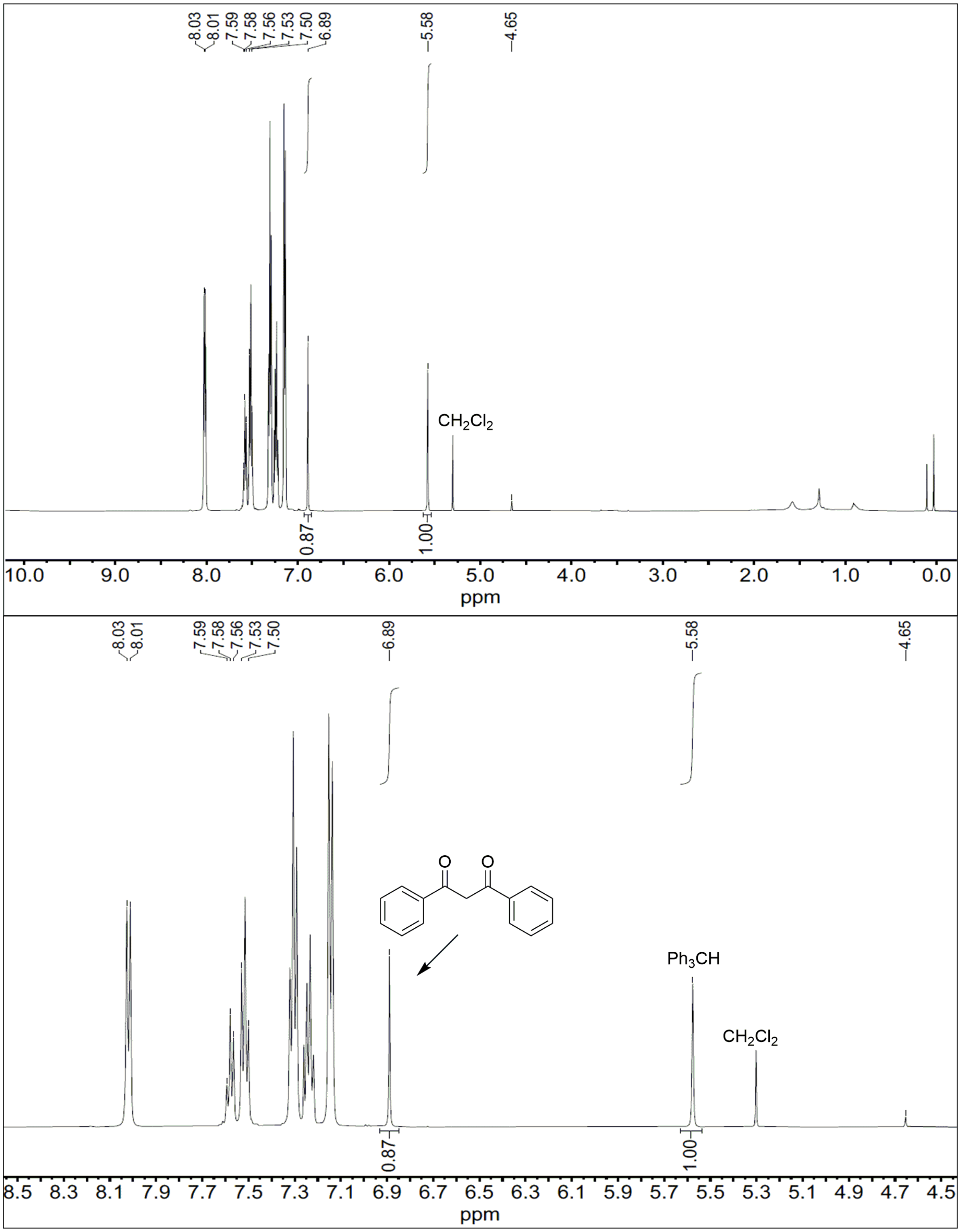

Figure S38. ^{1}H NMR (CD_3CN) of the organic recovery from the reaction mixture of in-situ generated **3**. Ph_3CH is present as an internal standard.

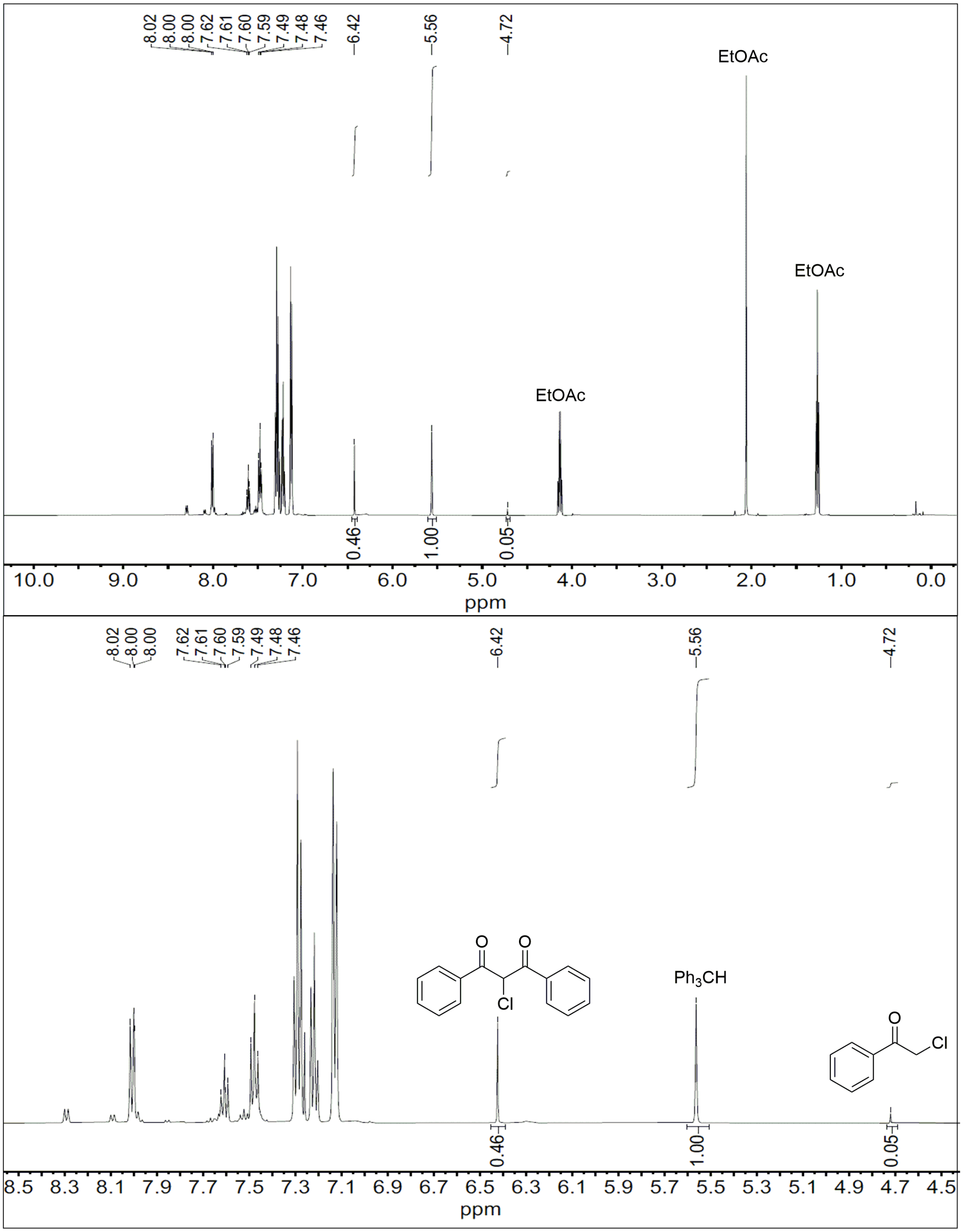

Figure S39. ^{1}H NMR (CD_3CN) of the organic recovery from the reaction mixture of **7** under O_2. Ph_3CH is present as an internal standard.

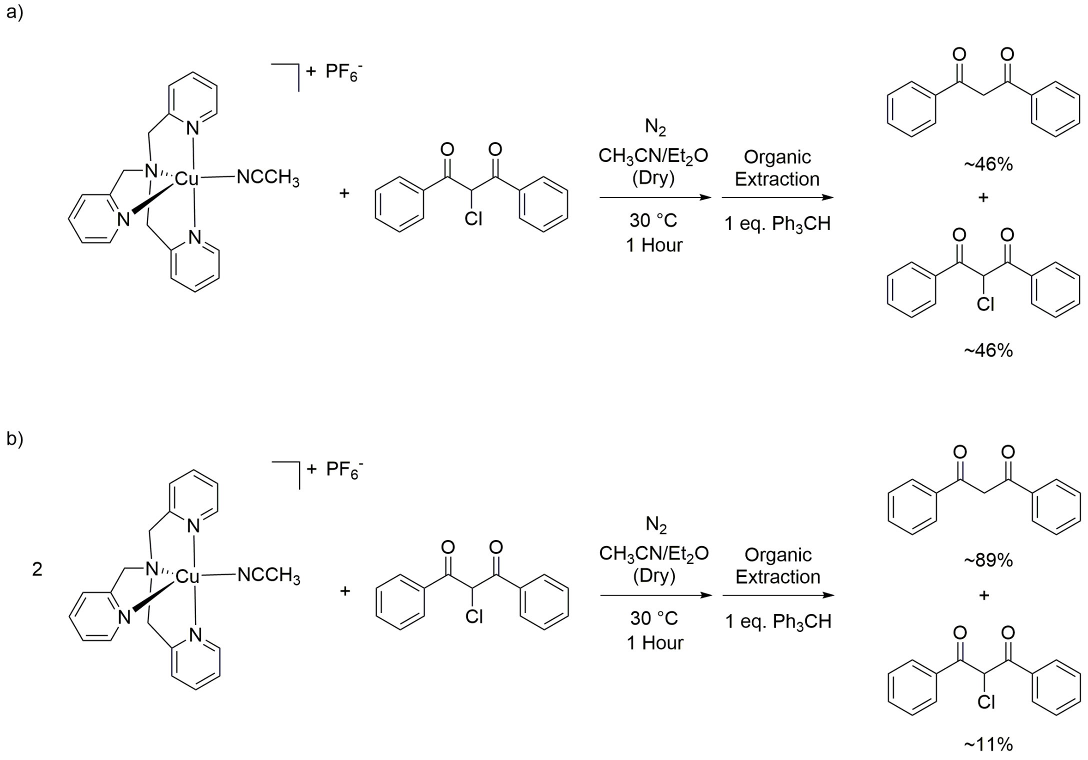

Scheme S1. General reaction for dehalogenation of 2-chloro-1,3-diphenyl-1,3-propanedion by 1 eq (a) or 2 eq (b) of [(TPA)Cu(CH_3CN)]PF_6.

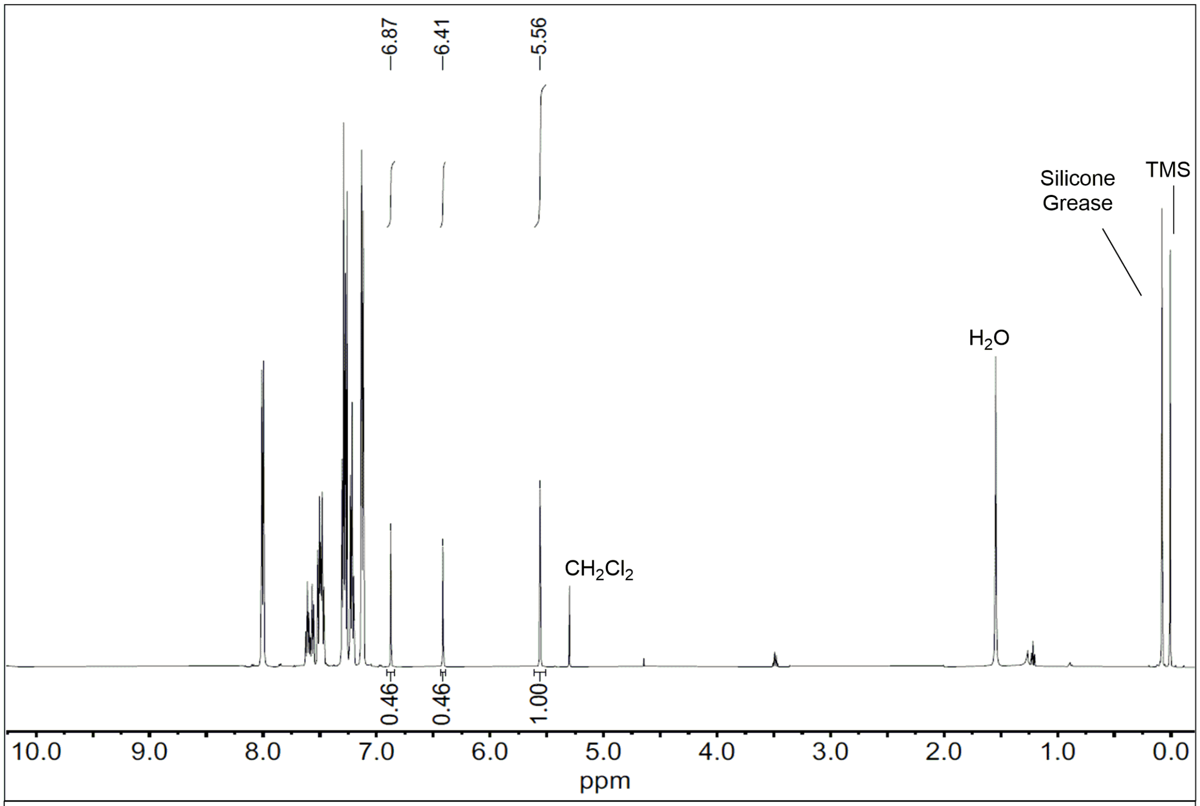

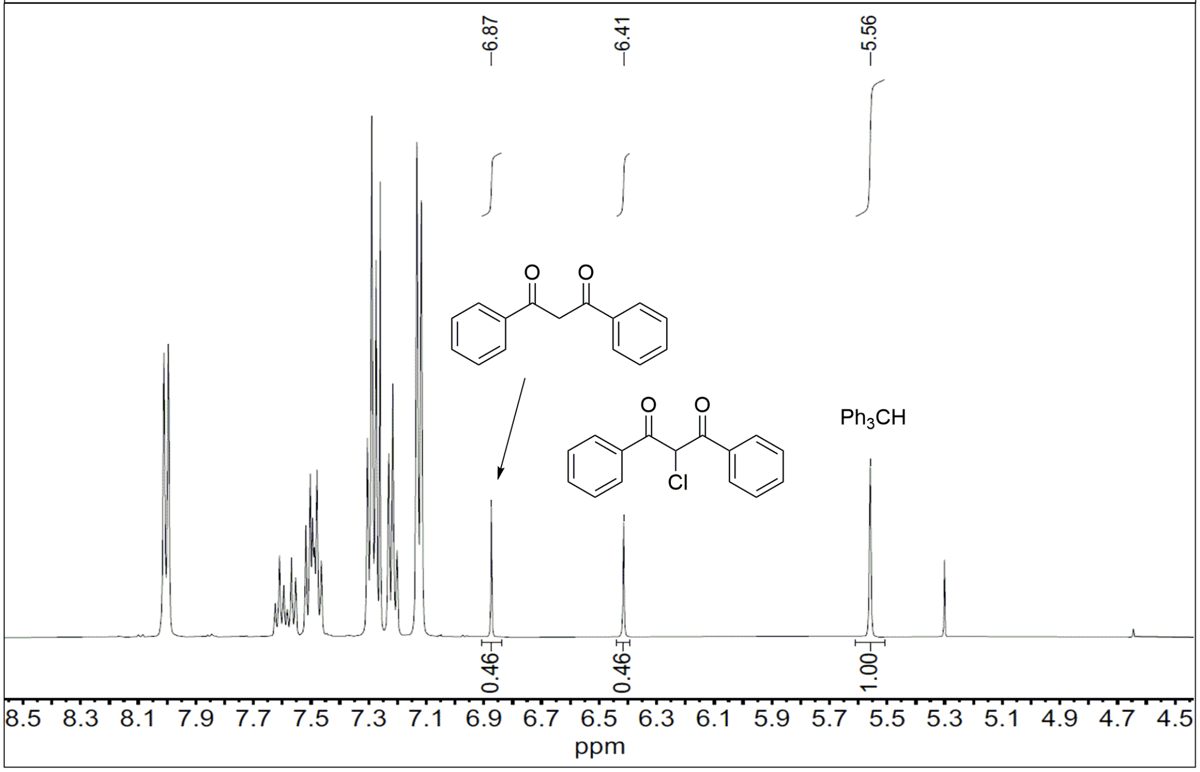

Figure S40. ^{1}H NMR (CD_3CN) of the organic recovery following reaction of $[(TPA)Cu(CH_3CN)]PF_6$ (1 eq) with 2-chloro-1,3-phenylpropane-1,3-dione (1 eq). Ph_3CH is present as an internal standard.

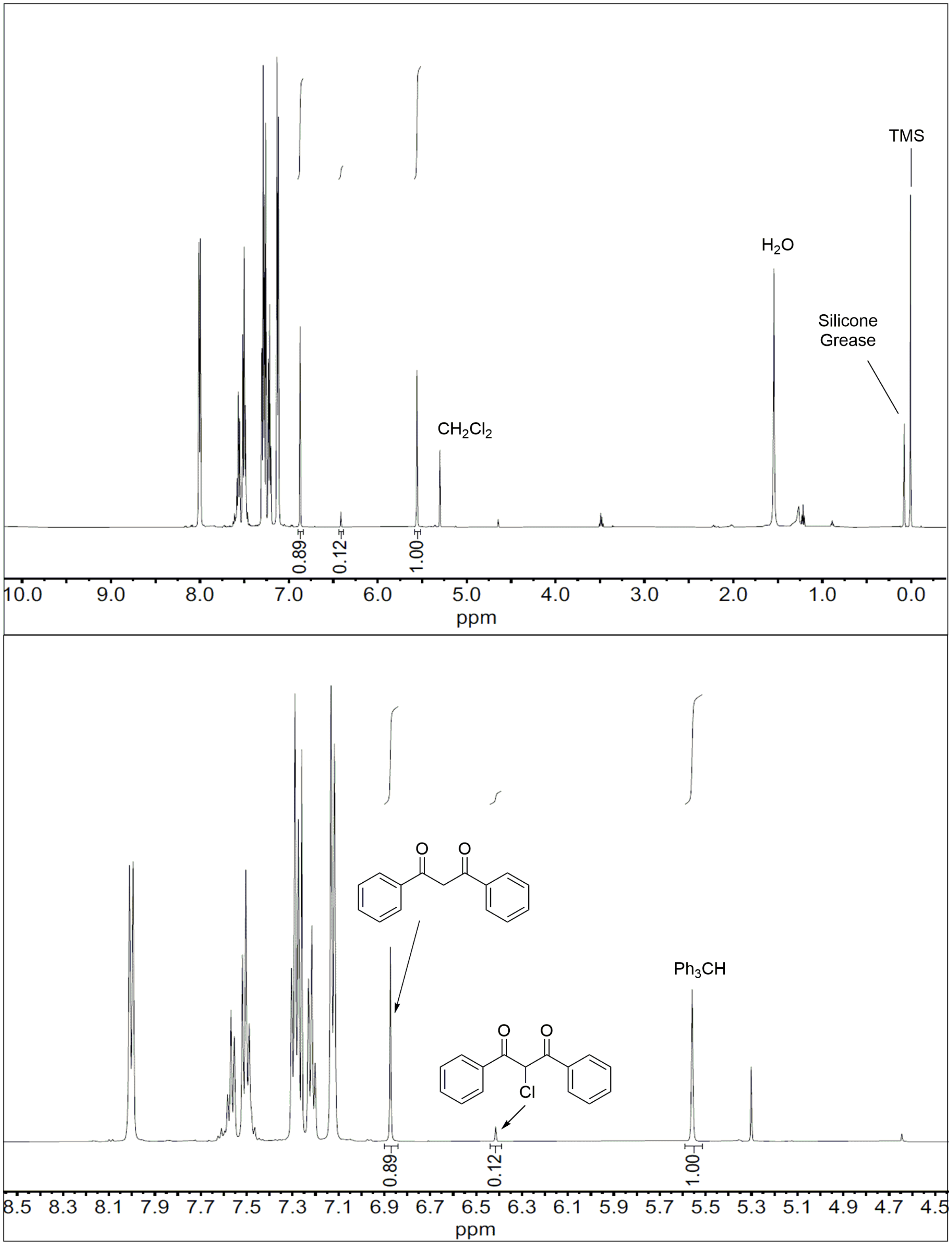

Figure S41. ^{1}H NMR (CD_3CN) of the organic recovery following reaction of [(TPA)Cu(CH_3CN)]PF_6 (2 eq) with 2-chloro-1,3-phenylpropane-1,3-dione (1 eq). Ph_3CH is present as an internal standard.

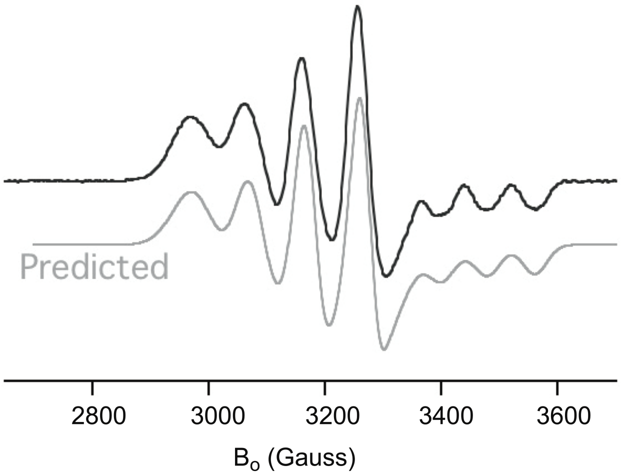

Figure S42. EPR spectrum of $[(TPA)Cu(O_2CPh)]ClO_4$ (**12**) in CH_2CH_2:toluene (1:1) at 4.5 K and a simulated spectrum**.** This complex exhibits a strained EPR spectrum that is dominated by a much more isotropic $^{63,65}Cu$ hyperfine tensor; $[A_{||}, A_{\perp}]$ = [285, 220] MHz. Simulations show that the observed line shape can be matched without including any ^{14}N couplings, with the inclusion of an isotropic g-strain of 0.02 and 90 MHz of A-strain (parallel direction only).

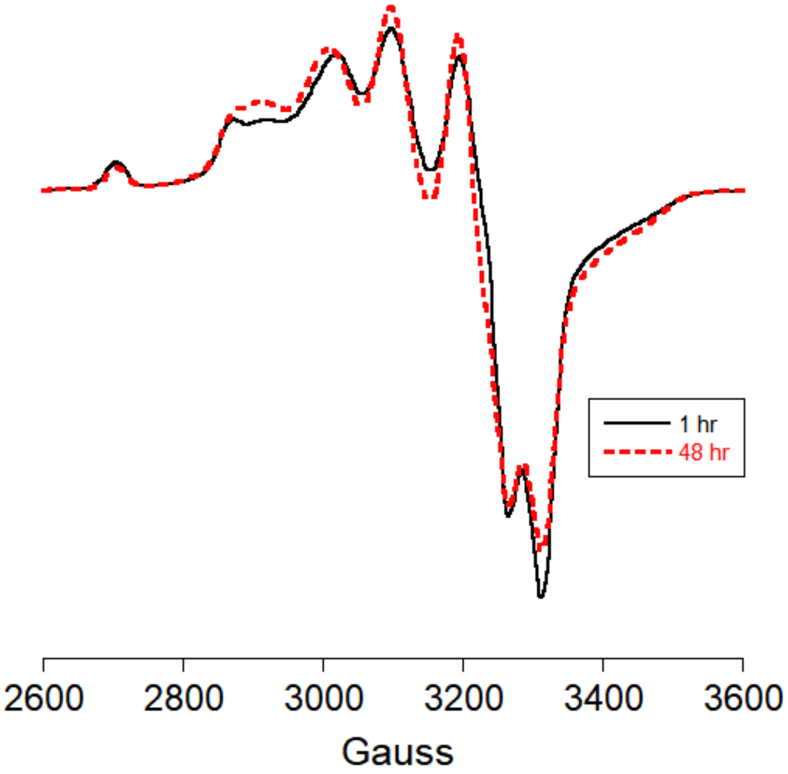

Figure S43. EPR spectra of the reaction mixture of **8** after stirring for 1 hr (black) and 48 hr (red), respectively, at 30 °C. The samples were collected in CH_3CN:toluene (1:1) at 12 K **.**

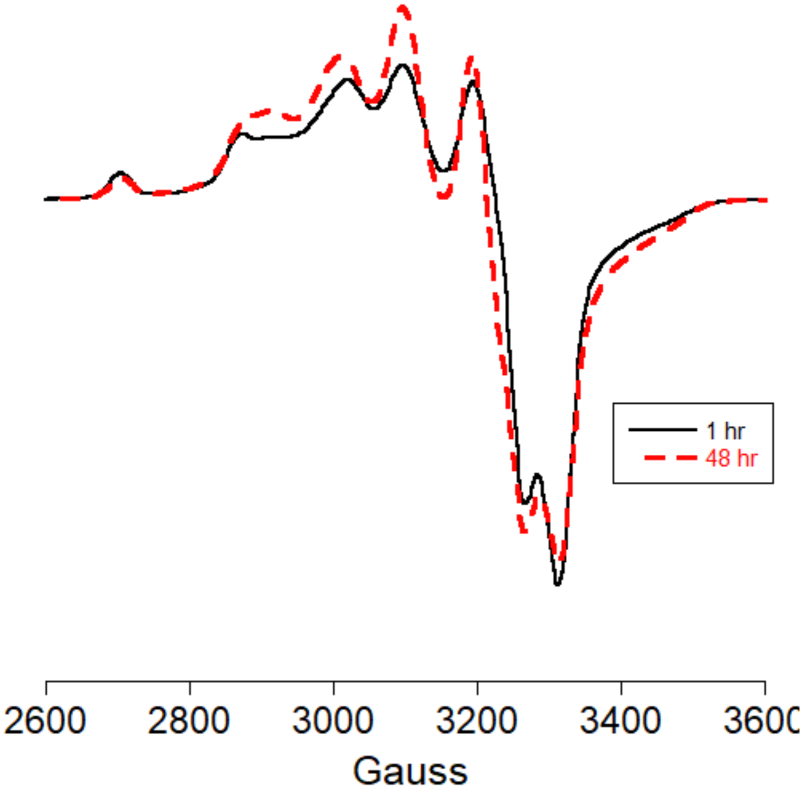

Figure S44. EPR spectra of the reaction mixture of **9** after stirring for 1 hr (black) and 48 hr (red), respectively, at 30 °C. The samples were collected in CH_3CN:toluene (1:1) at 12 K **.**

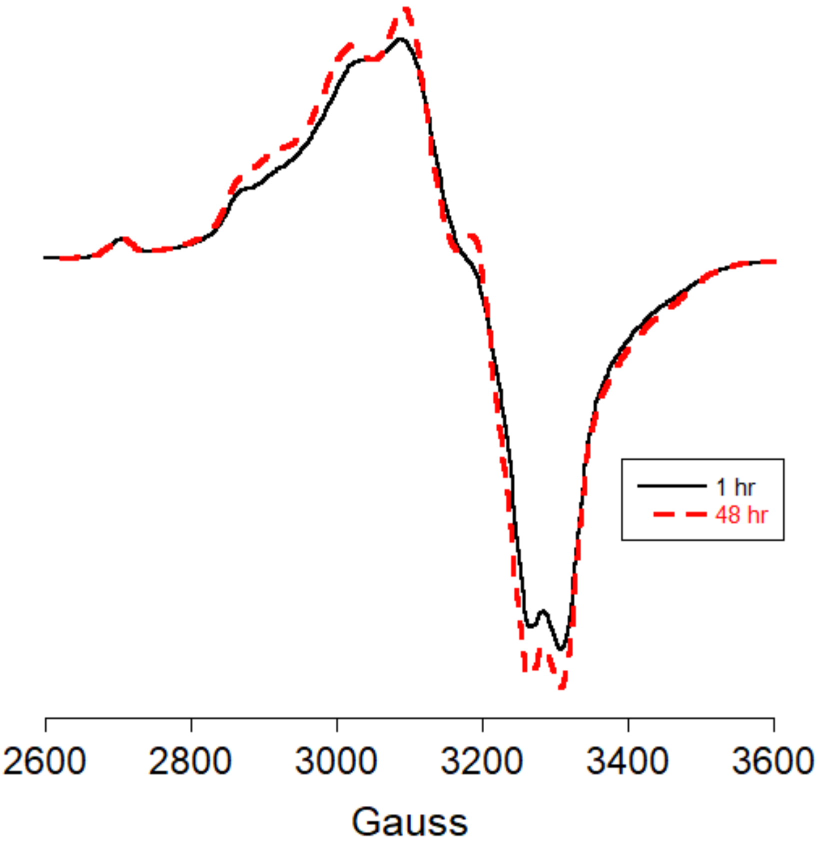

Figure S45. EPR spectra of the reaction mixture of **10** (R = -Cl) after stirring for 1 hr (black) and 48 hr (red), respectively, at 30 °C. The samples were collected in CH_3CN:toluene (1:1) at 12 K**.**

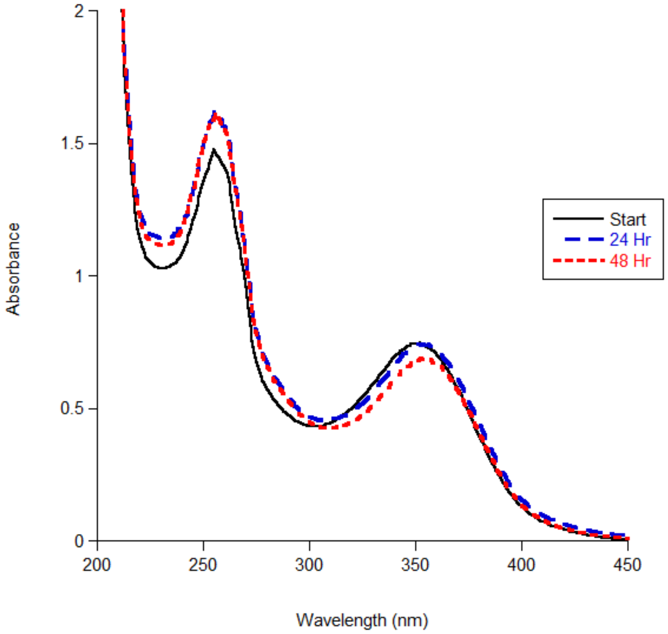

Figure S46. Absorption spectra (CH_3CN) of the reaction mixture of **7** at the start of the reaction, and after 24 and 48 h.

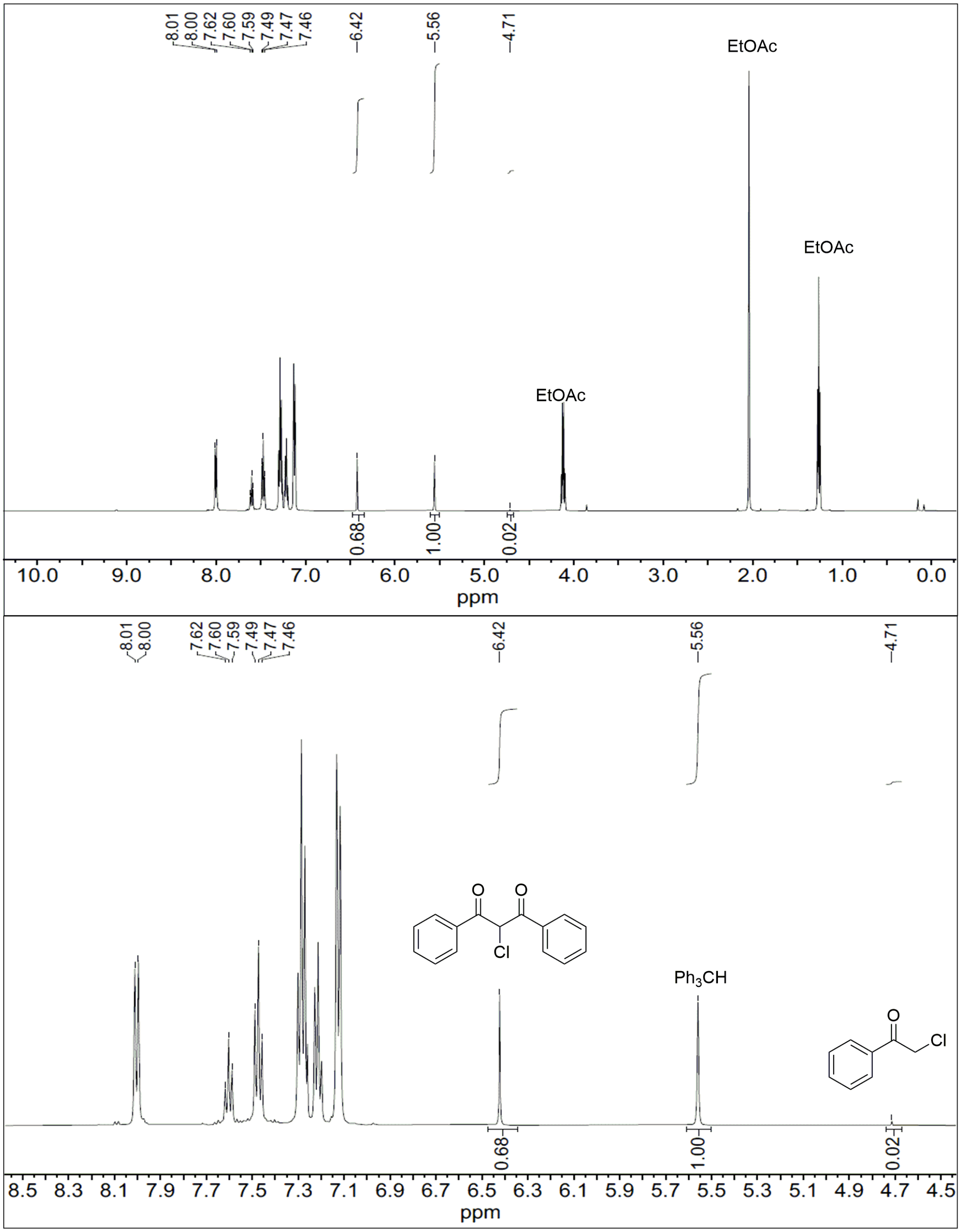

Figure S47. ^{1}H NMR (CD_3CN) of the organic recovery from the reaction mixture of **7** after 1 hr. Ph_3CH is present as an internal standard.

Table S1. Summary of X-ray data collection and refinement for **3-6.**

	3	**4**	**5**	**6**
empirical formula	$C_{66}H_{58}Cl_2Cu_2N_8O_{12}$	$C_{35}H_{33}ClCuN_4O_6$	$C_{35}H_{33}ClCuN_4O_8$	$C_{66}H_{54}Cl_6Cu_2N_8O_{12}$
formula weight	1353.18	704.64	736.64	1490.95
crystal system	Triclinic	Monoclinic	Monoclinic	Monoclinic
space group	*P*-1	$P2_1/c$	$P2_1/c$	$P2_1$
a (Å)	10.6383(5)	12.8484(7)	12.6105(4)	12.4169(3)
b (Å)	16.6917(8)	21.3956(12)	22.0545(6)	21.7754(5)
x (Å)	18.4503(9)	12.5769(6)	12.8161(4)	12.5537(4)
α (deg)	77.820(2)	90	90	90
β (deg)	80.769(2)	113.825(2)	114.532(4)	113.723(4)
γ (deg)	71.530(2)	90	90	90
V (Å^3)	3022.0(3)	3162.8(3)	3242.63(19)	3107.49(17)
Z	4	4	4	2
density (calcd), Mg m^{-3}	1.487	1.480	1.509	1.593
temp (K)	100(1)	100	100 (2)	100 (1)
crystal size (mm^3)	0.03 x 0.09 x 0.11	0.41 x 0.12 x 0.06	0.09 x 0.30 x 0.39	0.777 x 0.23 x 0.114
diffractometer	Bruker D8 Venture	Bruker D8 Venture	XtaLAB Synergy-S	Rigaku
Abs. coeff. (mm^{-1})	0.864	0.829	0.817	1.017
2θ max (deg)	54.79	54.98	64.82	61.49
Reflections collected	9807	65958	13931	15300
Indep. reflections	13934	7271	6625	18046
variable parameters	811	448	444	849
*R*1 / w*R*2[b]	0.0371/0.0782	0.0850/0.1653	0.0330/0.0839	0.0506/0.1253
goodness-of-fit (F^2)	1.032	1.344	1.048	1.017
largest diff. (e Å^{-3})	0.608/-0.526	0.69/-0.91	0.722/-0.483	1.47/-1.92

[a] Radiation used: Mo Kα (λ = 0.71073 Å). [b] $R1 = \sum \mid |F_o| - |F_c| \mid / \sum |F_o|$;
$wR2 = [\sum[w(F_o^2-F_c^2)^2]/[\sum(F_o^2)^2]]^{1/2}$ where $w = 1/[\sigma^2(F_o^2) + (aP)^2 + bP]$.

Table S2. Selected bond distances (Å) and angles (deg) for **3** and **4**.

	3		**4**
	Cation A	**Cation B**	
Cu(1)-O(1)	1.9384(14)	1.9443(13)	1.937(3)
Cu(1)-O(2)	1.9391(14)	1.9218(13)	1.943(3)
Cu(1)-N(1)	2.0981(17)	2.0954(16)	2.062(4)
Cu(1)-N(2)	2.0122(17)	1.9992(16)	1.994(4)
Cu(1)-N(3)	2.3561(18)	2.3481(18)	2.831
Cu(1)-N(4)	2.3680(19)	2.4945(17	2.274(4)
O(1)-C(19)	1.274(2)	1.279(2)	1.283(5)
O(2)-C(27)	1.277(2)	1.280(2)	-
O(2)-C(28)	-	-	1.282(5)
O(1)-Cu(1)-O(2)	92.99(6)	92.87(6)	92.71(13)
O(1)-Cu(1)-N(1)	89.47(6)	93.39(6)	174.11(14)
O(1)-Cu(1)-N(2)	172.69(7)	175.10(6)	92.51(14)
O(1)-Cu(1)-N(3)	94.54(6)	88.21(6)	111.46
O(1)-Cu(1)-N(4)	83.44(6)	93.05(6)	98.13(14)
O(2)-Cu(1)-N(1)	175.47(6)	172.48(6)	91.01(14)
O(2)-Cu(1)-N(2)	93.52(6)	90.37(6)	167.58(14)
O(2)-Cu(1)-N(3)	97.17(6)	100.89(6)	91.02
O(2)-Cu(1)-N(4)	108.45(6)	106.88(6)	93.03(14)
N(1)-Cu(1)-N(3)	78.83(6)	75.15(6)	73.01
N(1)-Cu(1)-N(4)	75.60(6)	76.94(6)	77.10(15)
N(2)-Cu(1)-N(1)	83.82(7)	83.66(6)	84.75(15)
N(2)-Cu(1)-N(3)	81.33(6)	94.79(6)	76.20
N(2)-Cu(1)-N(4)	97.65(6)	82.49(6)	97.37(15)
N(3)-Cu(1)-N(4)	154.36(6)	152.09(6)	149.84

Table S3. Selected bond distances (Å) and angles (deg) for **5**.

	5
Cu(1)-O(1)	1.9325(13)
Cu(1)-O(2)	1.9234(13)
Cu(1)-N(1)	2.0586(15)
Cu(1)-N(2)	2.2994(16)
Cu(1)-N(3)	1.9868(15)
Cu(1)-N(38)*	2.79
O(1)-C(19)	1.278(2)
O(2)-C(28)	1.285(2)
O(1)-Cu(1)-O(2)	92.10(5)
O(1)-Cu(1)-N(1)	91.35(6)
O(1)-Cu(1)-N(2)	90.73(6)
O(1)-Cu(1)-N(3)	168.23(6)
O(1)-Cu(1)-N(38)	90.37
O(2)-Cu(1)-N(1)	175.26(6)
O(2)-Cu(1)-N(2)	99.41(6)
O(2)-Cu(1)-N(3)	92.95(6)
O(2)-Cu(1)-N(38)	108.57
N(1)-Cu(1)-N(3)	84.27(6)
N(1)-Cu(1)-N(38)	74.63
N(2)-Cu(1)-N(1)	77.29(6)
N(2)-Cu(1)-N(3)	98.91(6)
N(2)-Cu(1)-N(38)	151.92
N(3)-Cu(1)-N(38)	77.95

Table S4. Selected bond distances (Å) and angles (deg) for **6**

	6	
	Cation A	**Cation B**
Cu(1)-O(1)	1.927(3)	1.924(3)
Cu(1)-O(2)	1.947(3)	1.949(3)
Cu(1)-N(1)	2.058(4)	2.043(4)
Cu(1)-N(2)	1.985(3)	1.982(3)
Cu(1)-N(3)	2.264(4)	2.262(4)
Cu(1)-N(4)	2.754	2.876
O(1)-C(19)	1.283(5)	1.292(5)
O(2)-C(27)	1.272(5)	1.280(5)
O(1)-Cu(1)-O(2)	92.22(13)	92.36(13)
O(1)-Cu(1)-N(1)	172.72(14)	175.01(15)
O(1)-Cu(1)-N(2)	93.02(14)	93.40(14)
O(1)-Cu(1)-N(3)	95.74(14)	98.49(13)
O(1)-Cu(1)-N(4)	113.01	110.73
O(2)-Cu(1)-N(1)	91.41(13)	90.85(14)
O(2)-Cu(1)-N(2)	166.78(14)	166.83(14)
O(2)-Cu(1)-N(3)	94.25(14)	91.59(13)
O(2)-Cu(1)-N(4)	90.45	92.80
N(1)-Cu(1)-N(3)	77.69(14)	77.59(14)
N(1)-Cu(1)-N(4)	73.26	72.90
N(2)-Cu(1)-N(1)	84.80(14)	84.27(15)
N(2)-Cu(1)-N(3)	97.29(14)	99.25(15)
N(2)-Cu(1)-N(4)	76.32	74.08
N(3)-Cu(1)-N(4)	150.67	150.22

Table S5. Summary of X-ray data collection and refinement for **11**

	11
empirical formula	$C_{38}H_{39}Cl_5Cu_2LiN_9O_{12}$
formula weight	1125.06
crystal system	Trigonal
space group	*P3c1*
a (Å)	12.6221(10)
b (Å)	12.6221(10)
x (Å)	16.3066(12)
α (deg)	90
β (deg)	90
γ (deg)	120
V (Å^3)	2249.9(4)
Z	1.99998
density (calcd), Mg m^{-3}	1.661
temp (K)	100
crystal size (mm^3)	0.11 x 0.12 x 0.20
diffractometer	Bruker D8 Venture
Abs. coeff. (mm^{-1})	1.314
2θ max (deg)	60.902
Reflections collected	9941
Indep. reflections	3427
variable parameters	334
$R1$ / w$R2^b$	0.0386/0.0850
goodness-of-fit (F^2)	1.023
largest diff. (e Å^{-3})	0.671/-0.285

[a]Radiation used: Mo Kα (λ = 0.71073 Å). [b]$R1 = \sum | |F_o| - |F_c| | / \sum |F_o|$; w$R2 = [\sum[w(F_o^2-F_c^2)^2]/[\sum(F_o^2)^2]]^{1/2}$ where $w = 1/[\sigma^2(F_o^2) + (aP)^2 + bP]$.

Table S6. Selected bond distances (Å) and angles (deg) for **11**

	11	
	Cation A	**Cation B**
Cu(1)-Cl(1)	2.234(2)	2.238(2)
Cu(1)-N(1)	2.063(3)	2.055(3)
Cu(1)-N(2)	2.068(7)	2.035(8)
N(1)-Cu(1)-Cl(1)	99.26(10)	98.75(9)
N(1)-Cu(1)-N(1)	117.46(5)	117.73(5)
N(1)-Cu(1)-N(2)	80.74(10)	81.25(9)
N(2)-Cu(1)-Cl(1)	180.0	180.0

Table S7. Summary of X-ray data collection and refinement for $[(TPA)Cu(O_2CPh)]ClO_4$ (**12**)

	$[(TPA)Cu(O_2CPh)]ClO_4$
empirical formula	$C_{25}H_{23}ClCuN_4O_6$
formula weight	574.46
crystal system	monoclinic
space group	$P2_1/c$
a (Å)	18.5496(10)
b (Å)	9.0884(5)
x (Å)	14.4320(7)
α (deg)	90
β (deg)	99.219(2)
γ (deg)	90
V (Å^3)	2401.6(2)
Z	4
density (calcd), Mg m^{-3}	1.589
temp (K)	100
crystal size (mm^3)	0.28 × 0.25 × 0.05
diffractometer	Bruker D8 Venture
Abs. coeff. (mm^{-1})	1.071
2θ max (deg)	54.260
Reflections collected	9904
Indep. reflections	5541
variable parameters	204
$R1$ / w$R2^b$	0.0396/0.0663
goodness-of-fit (F^2)	1.081
largest diff. (e Å^{-3})	0.50/-0.33

[a]Radiation used: Mo Kα (λ = 0.71073 Å). [b]$R1 = \sum \mid |F_o| - |F_c| \mid / \sum |F_o|$; w$R2 = [\sum[w(F_o^2-F_c^2)^2]/[\sum(F_o^2)^2]]^{1/2}$ where $w = 1/[\sigma^2(F_o^2) + (aP)^2 + bP]$.

Table S8. Selected bond distances (Å) and angles (deg) for [(TPA)Cu(O_2CPh)]ClO_4 (**12**)

	[(TPA)Cu(O_2CPh)]ClO_4 (**12**)
Cu(1)-O(1)	1.9384(13)
Cu(1)-N(1)	2.0295(14)
Cu(1)-N(2)	2.0340(15)
Cu(1)-N(3)	2.0794(15)
Cu(1)-N(4)	2.0983(15)
N(1)-Cu(1)-O(1)	176.95(6)
N(2)-Cu(1)-O(1)	100.67(6)
N(3)-Cu(1)-O(1)	98.97(6)
N(4)-Cu(1)-O(1)	96.38(5)
N(1)-Cu(1)-N(2)	81.15(6)
N(1)-Cu(1)-N(3)	81.81(6)
N(1)-Cu(1)-N(4)	80.60(6)
N(2)-Cu(1)-N(3)	125.56(6)
N(2)-Cu(1)-N(4)	115.86(6)
N(3)-Cu(1)-N(4)	111.63(6)